Metrology of Optical Systems

Figures and Images for Instructors

Module 3
Using Interferometry to Measure Precision Optics

Precision Optics Series

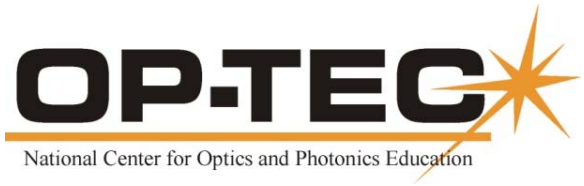

© 2018 University of Central Florida

This text was developed by the National Center for Optics and Photonics Education (OP-TEC), University of Central Florida, under NSF ATE grant 1303732. Any opinions, findings, and conclusions or recommendations expressed in this material are those of the author(s) and do not necessarily reflect the views of the National Science Foundation.

Published and distributed by
OP-TEC
University of Central Florida
http://www.op-tec.org

Permission to copy and distribute
This work is licensed under the Creative Commons Attribution-NonCommercial-NoDerivatives 4.0 International License. http://creativecommons.org/licenses/by-nc-nd/4.0. Individuals and organizations may copy and distribute this material for non-commercial purposes. Appropriate credit to the University of Central Florida & the National Science Foundation shall be displayed, by retaining the statements on this page.

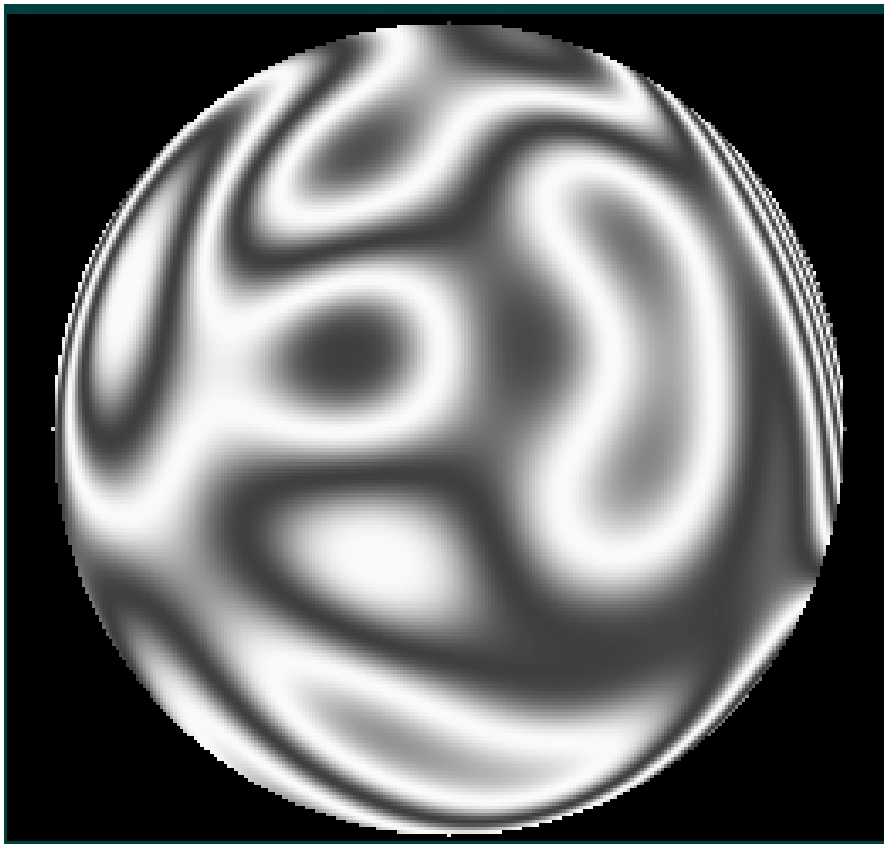

Figure 3-1 *The brightest regions are those of complete constructive interference, and the darkest regions are those of complete destructive interference, varying through all of the shades of lightness in between. When cast on a screen, the bright regions will be the color of the laser source used to create the interferogram and the dark regions will be dark. However, most interferometer detectors output fringe data as grayscale plots like this, or they might output false-color plots that grade the amount of OPD by color.*

$$d_e = \frac{R}{(k+1)}\left(1 \pm \sqrt{-k}\right) \quad for -1 < k < 0$$

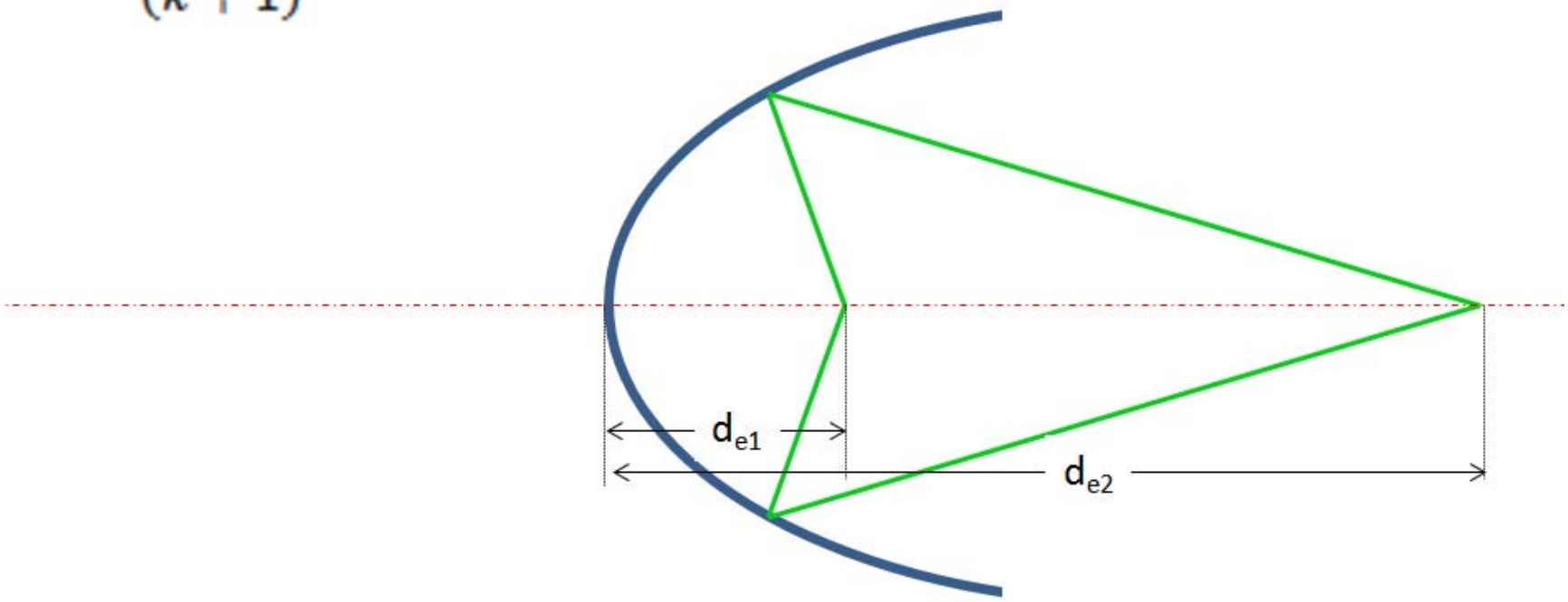

Figure 3-2 *The foci of an ellipsoid are located at d_{e1} and d_{e2}. Note that it is difficult to position a point source at one of these foci while retaining access to the other focus.*

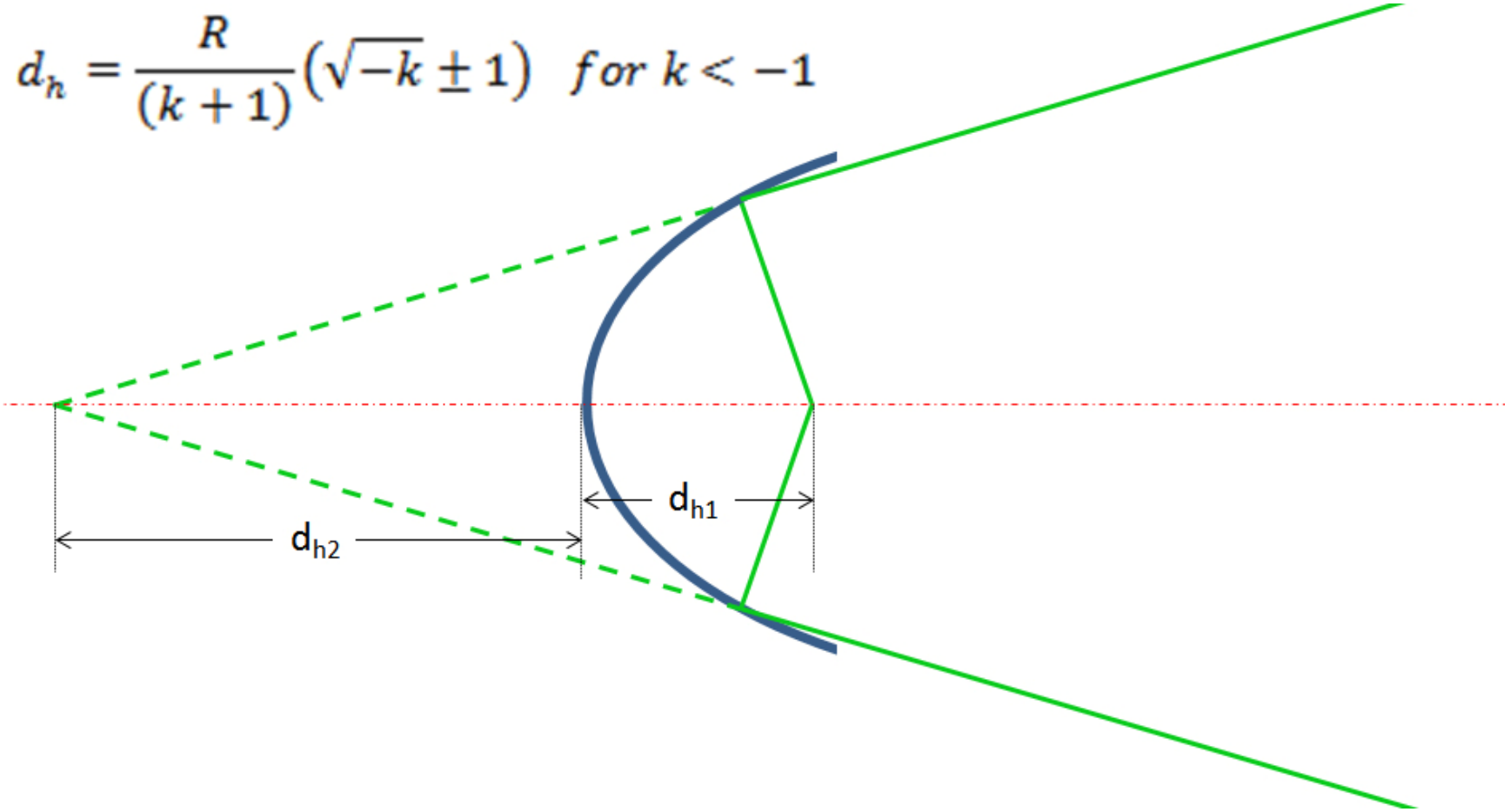

Figure 3-3 *The foci of a hyperboloid are located at d_{h1} and d_{h2}. Note that it is difficult to position a point source at one of these foci while retaining access to the other focus.*

$$d_p = \frac{R}{2} \quad for\ k = -1$$

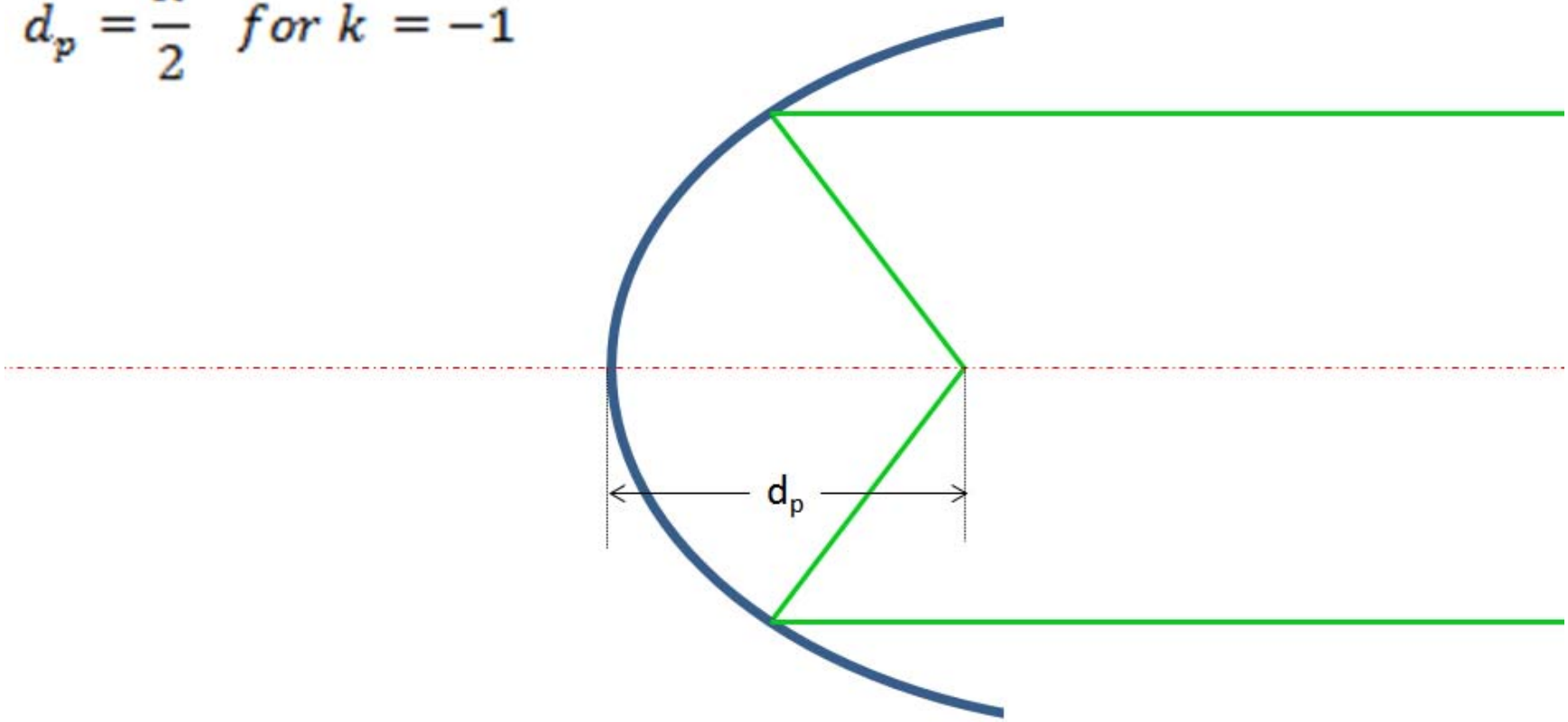

Figure 3-4 *The foci of a paraboloid are located at half the radius, R, of the best-fit sphere and at infinity. Note that a point source can be located at the finite focus and the paraboloid can be tested via the reflected, collimated light with only a minor obscuration of its clear aperture. Alternatively, a collimated input can be used to test a paraboloidal surface if the source is reflected by a spherical reflector centered at the paraboloid's finite focus.*

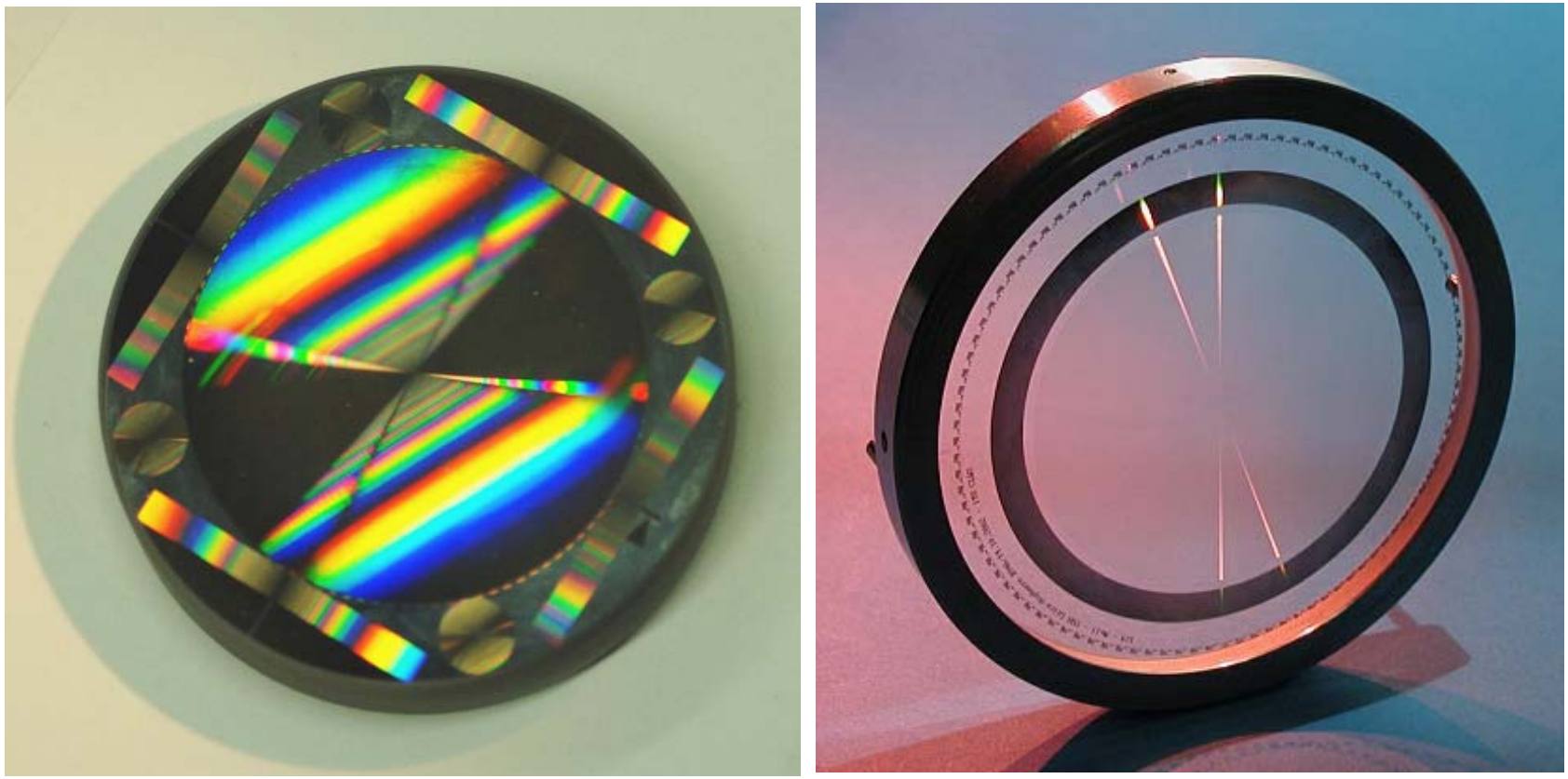

Figure 3-5 *These are photos of two different CGHs. These diffractive optical elements shape a reference beam in an interferometer application.*

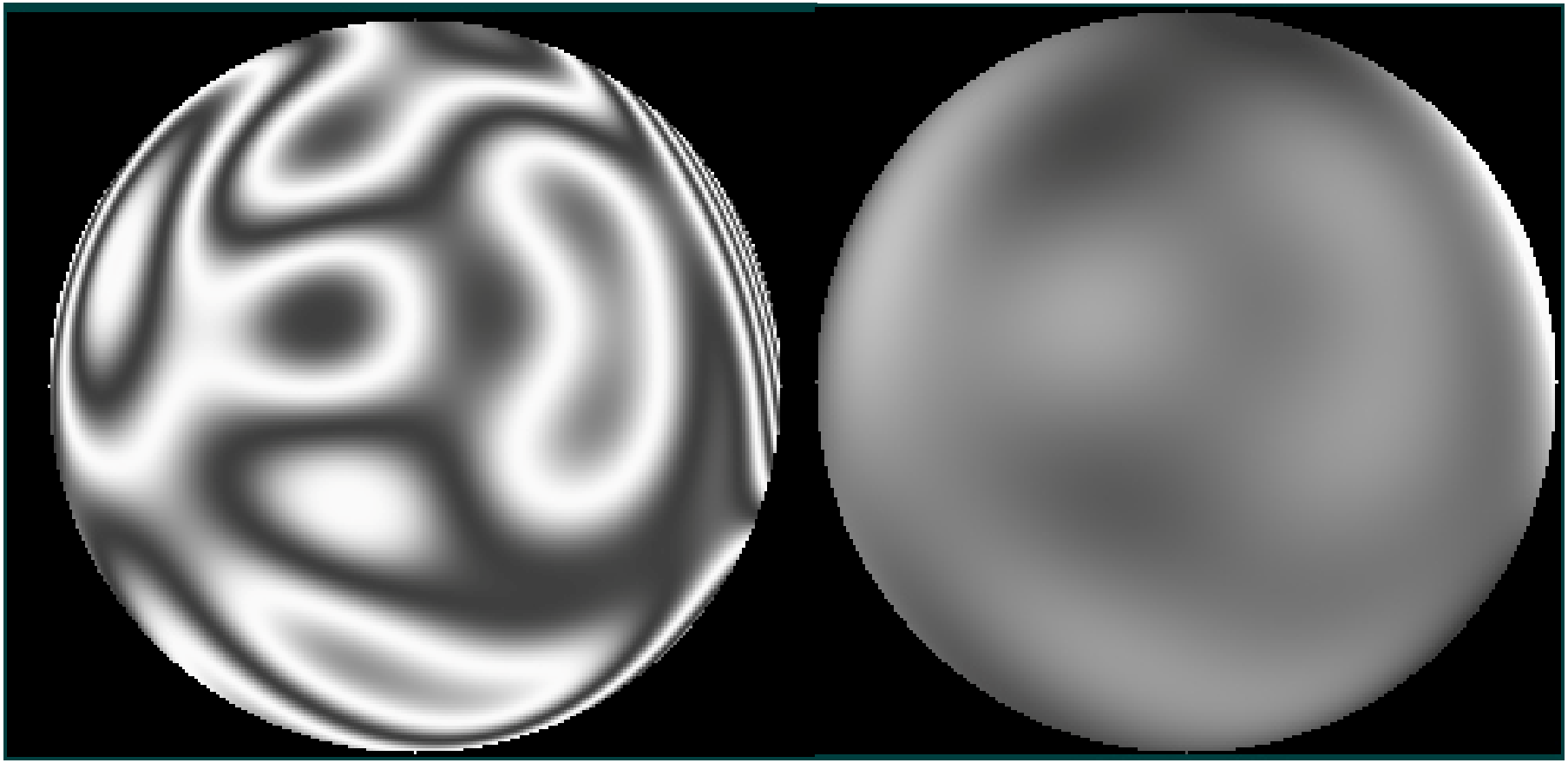

Figures 3-6a (left) and 3-6b (right) *The brightest regions now represent the highest parts of the wavefront or surface map, and the darkest regions represent the lowest parts of the map, varying through the shades of gray in between. However, most interferometer detectors output fringe data as false-color plots so that the shades of gray can be easily interpolated.*

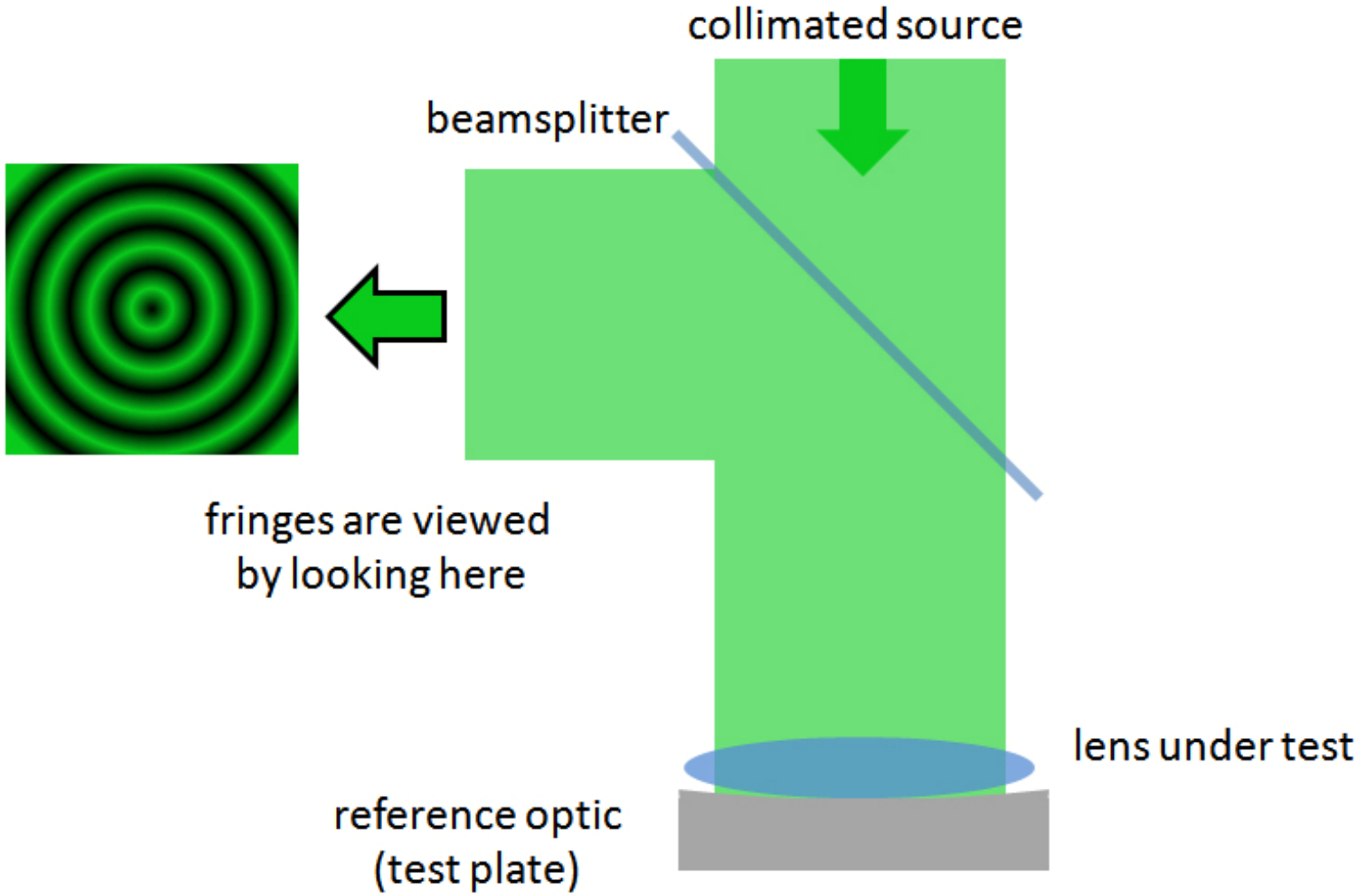

Figure 3-7 *As this schematic demonstrates, the Fizeau interferometer can be used to produce Newton's rings like those shown in the idealized interferogram.*

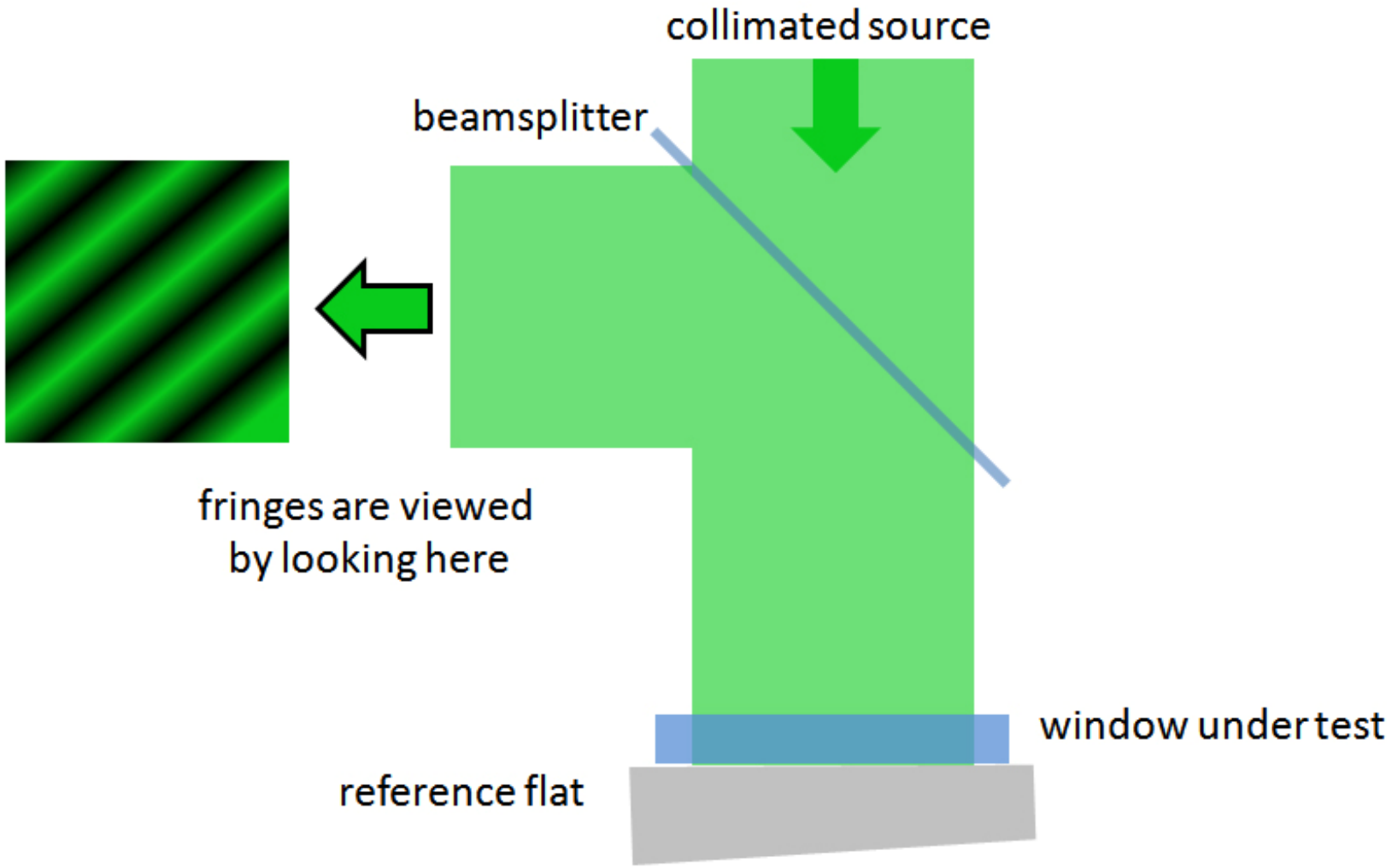

Figure 3-8 *As this schematic shows, the Fizeau interferometer can be used to test a window, producing linear fringes like those shown in the idealized interferogram. Figure 3-9 shows actual fringes*

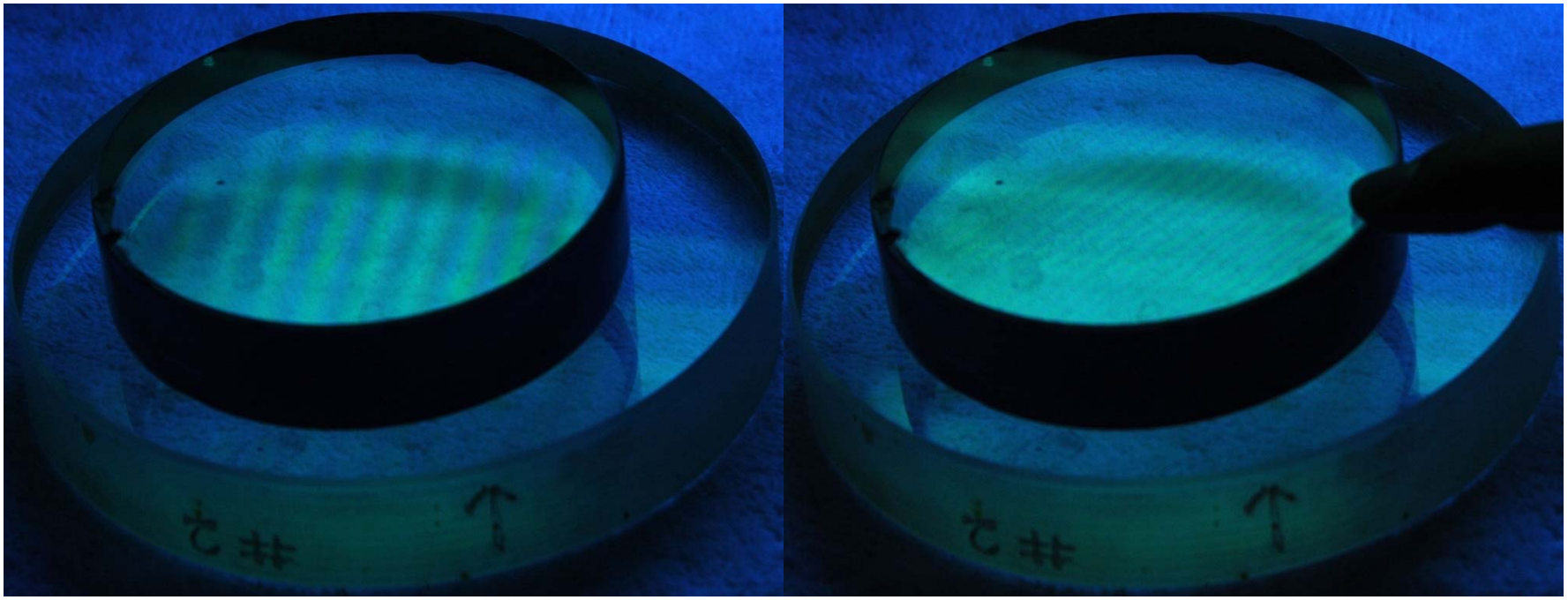

Figure 3-9 *These images show Newton's "rings" as parallel fringes between a calibrated reference flat and a (nearly) flat window. Additional tilt fringes are added in the figure on the right by lightly pressing on the optic under test. Additional fringes indicate that a greater optical path is created by pushing. If there was a surface-height defect of size h in the test surface, it would have created fringe deviation Δ, given fringe spacing S.*

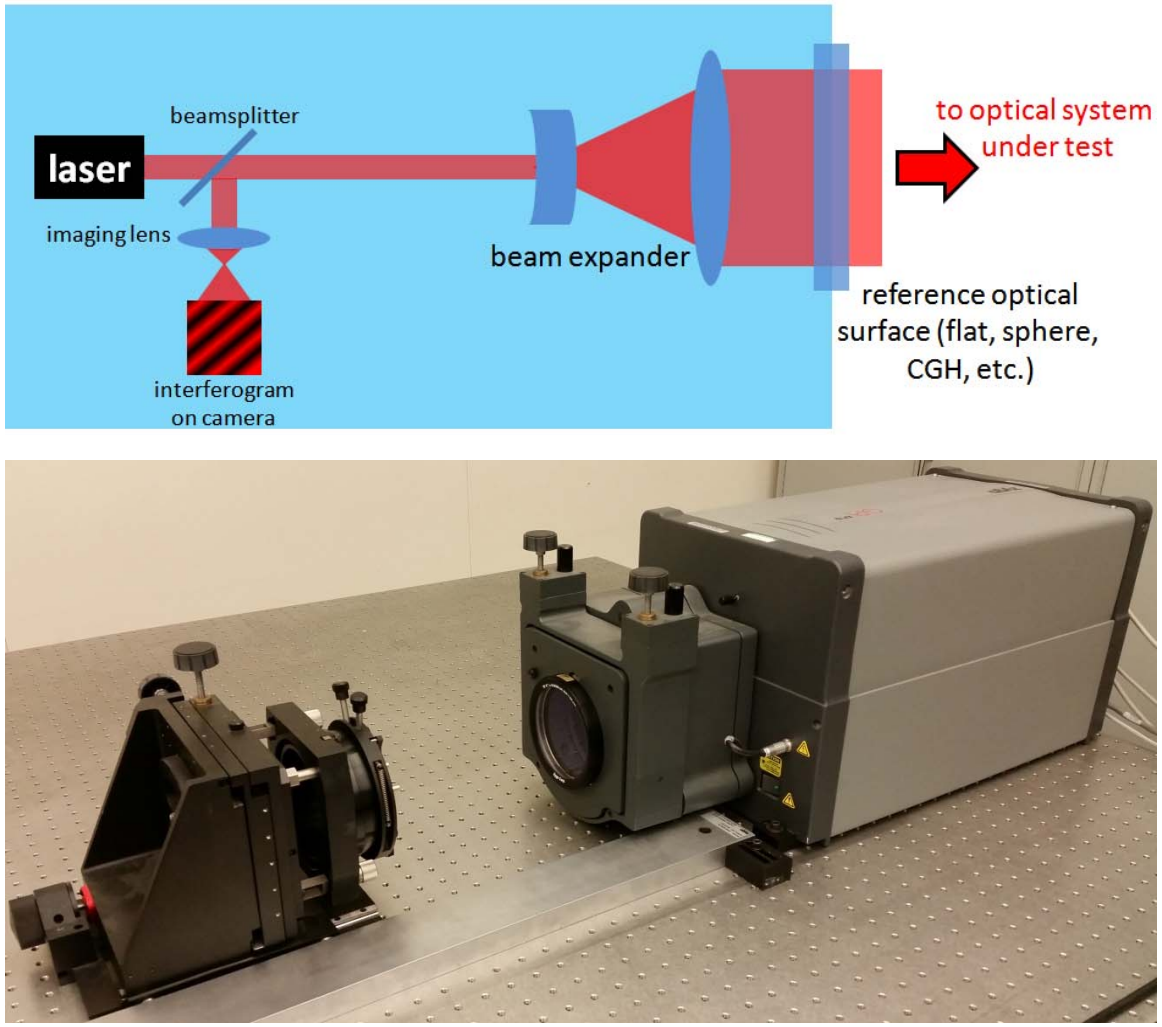

Figure 3-10 *The schematic (top) and the photograph (bottom) show that with a radial-slide module and three-point optic mount, the laser-based Fizeau interferometer can be used to test optical systems with long optical paths, even though the reference path is relatively short.*

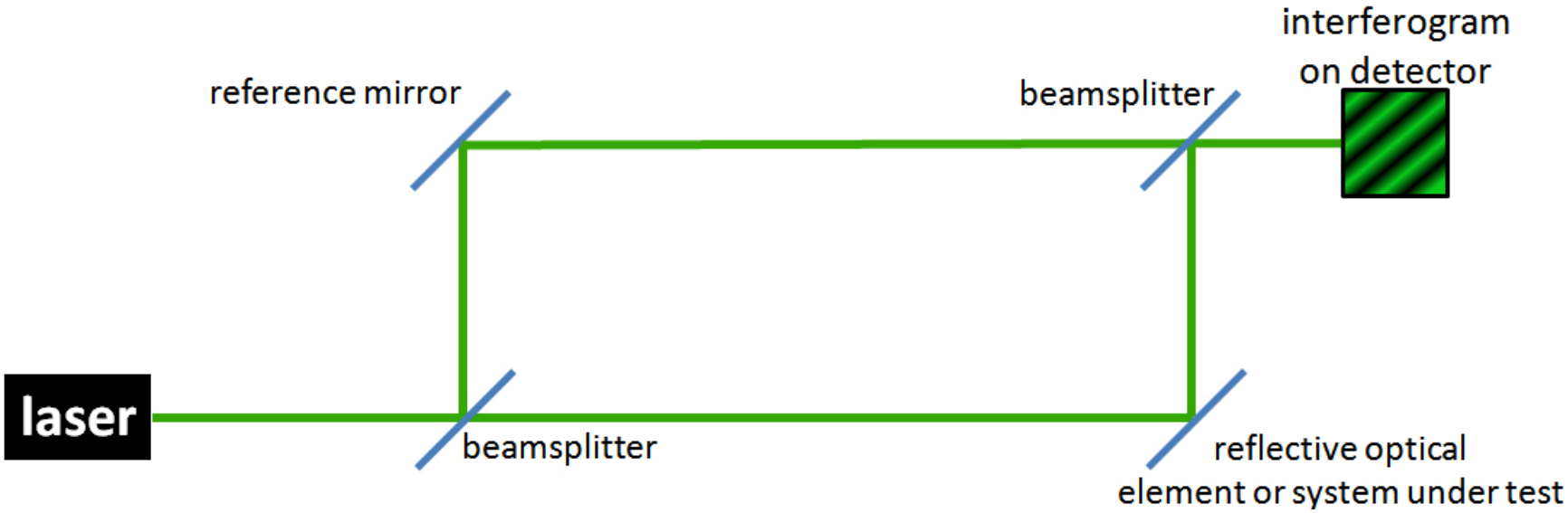

Figure 3-11 *This schematic shows a Mach-Zehnder interferometer used to test a reflective optical component or system.*

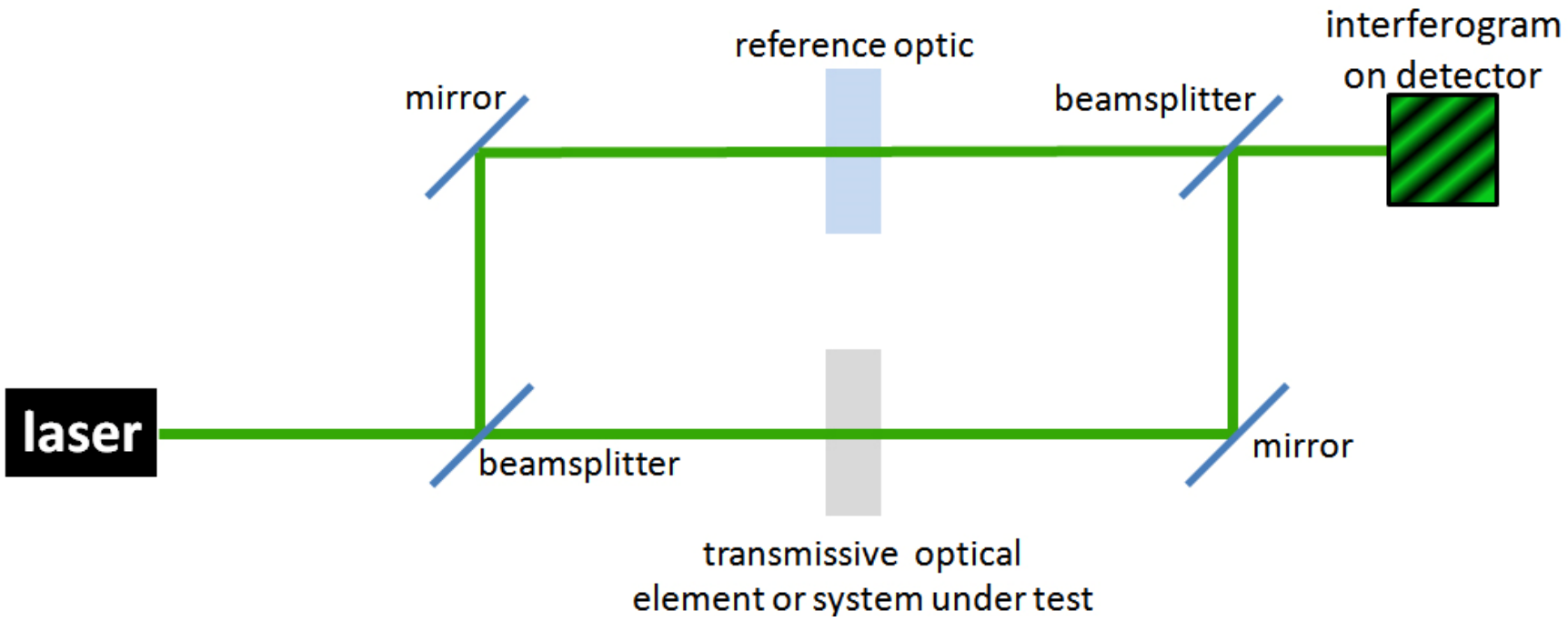

Figure 3-12 *This schematic shows a Mach-Zehnder interferometer used to test a transmissive optical component or system.*

optical property measured	optic tested	interferometric test setup	interferogram scale factor
reflected wavefront error (RWFE)	reflective optcal component	normal angle of incidence $\theta = 0$, single reflection (single pass)	$\lambda/2$
reflected wavefront error (RWFE)	reflective optical component	angle of incidence $\theta \neq 0$, single reflection (single pass)	$\lambda/(2\cdot\cos\theta)$
reflected wavefront error (RWFE)	reflective optical system	normal angle of incidence $\theta = 0$, double reflection (double pass)	$\lambda/4$
reflected wavefront error (RWFE)	reflective optical system	angle of incidence $\theta \neq 0$, double reflection (double pass)	$\lambda/(4\cdot\cos\theta)$
transmitted wavefront error (TWFE)	transmissive optical component	normal angle of incidence $\theta = 0$, single transmission (single pass)	λ
transmitted wavefront error (TWFE)	transmissive optical system	normal angle of incidence $\theta = 0$, double transmission (double pass)	$\lambda/2$

Figure 3-13 *This chart shows the scale factors for common interferometer setups.*

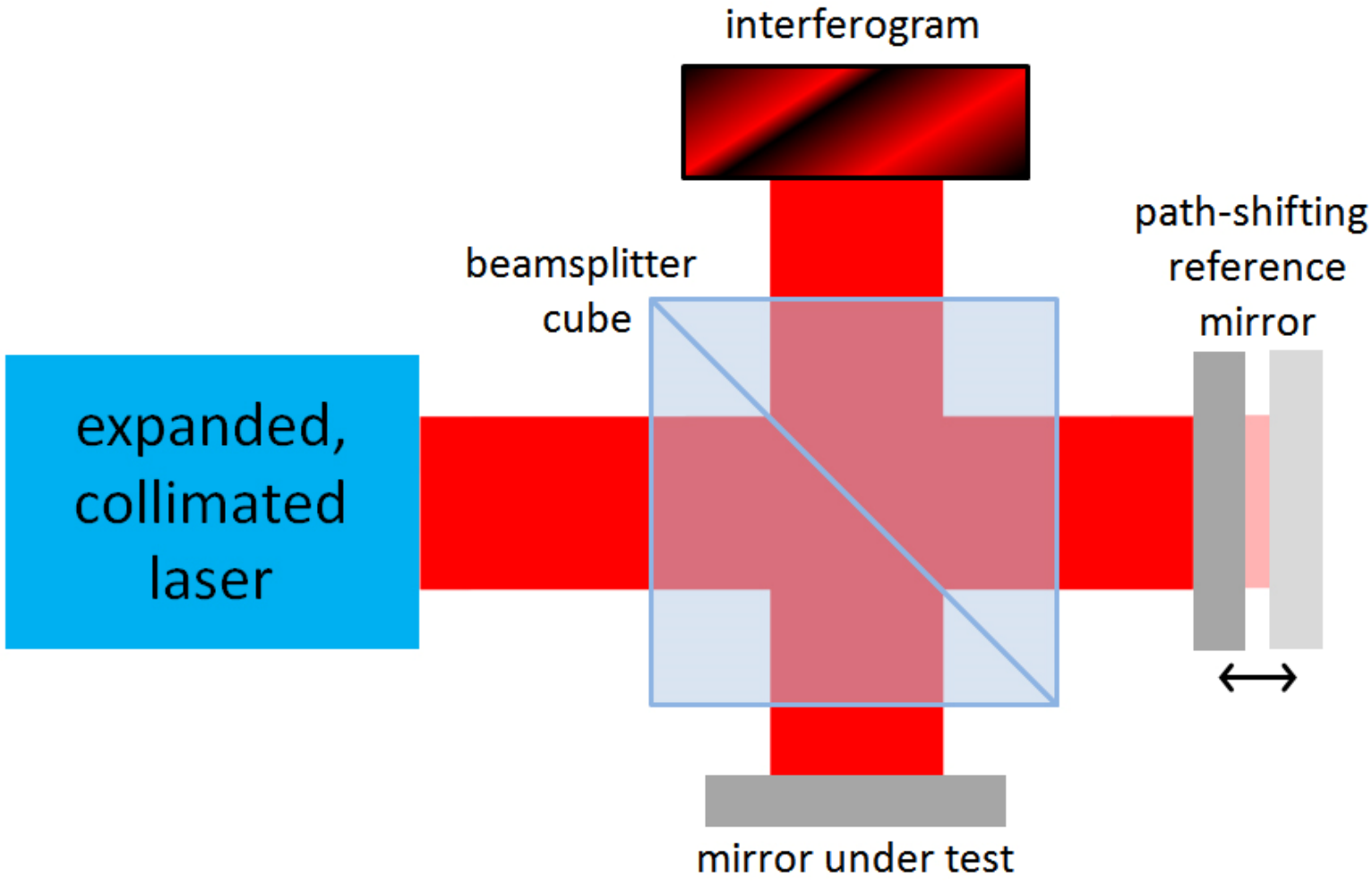

Figure 3-14 *The relatively simple layout of a Michelson interferometer usually uses an AR-coated cube beamsplitter. It can be applied in versatile ways, including as a sensor, where one arm of the interferometer may be used as the sensing element.*

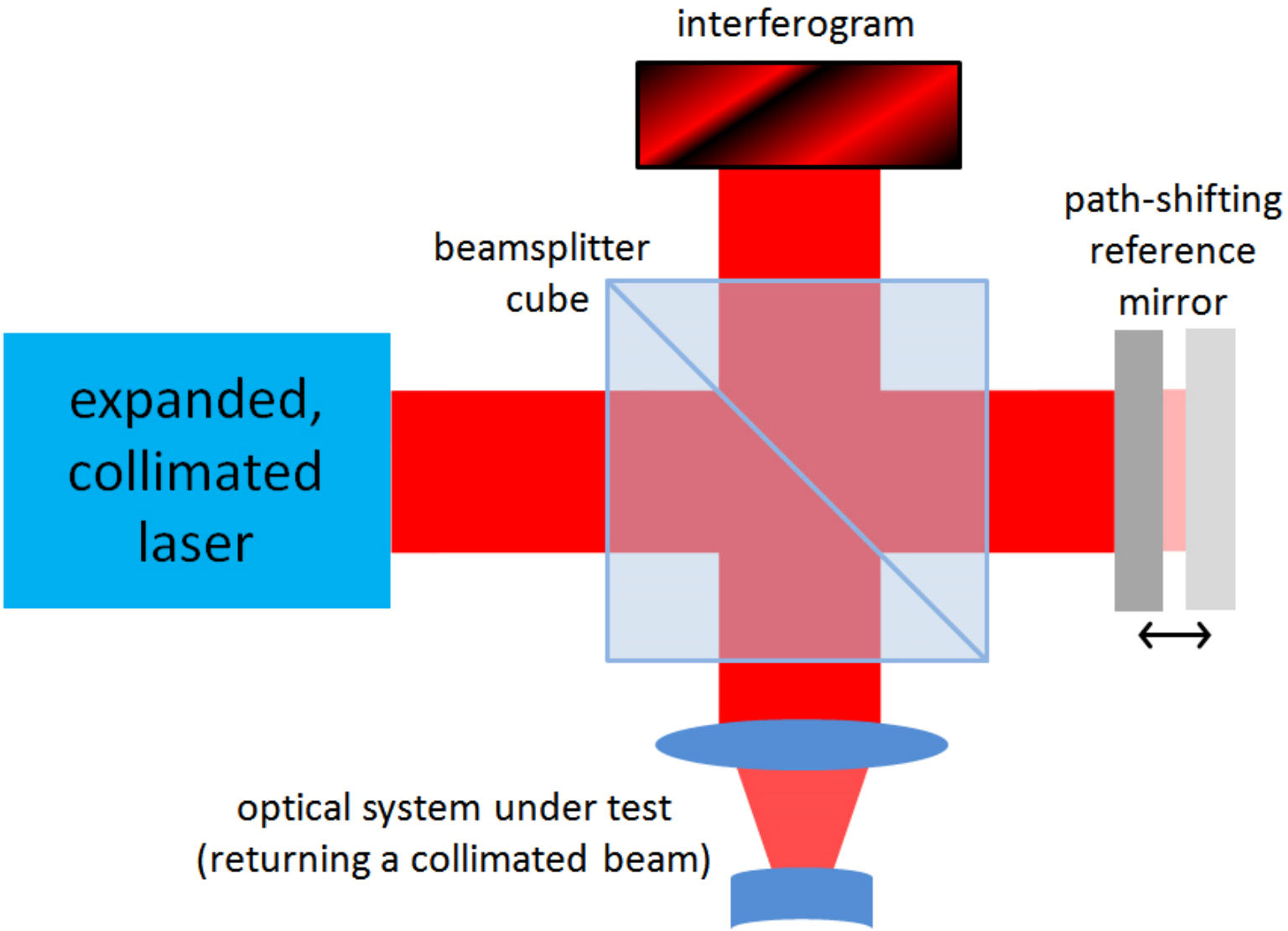

Figure 3-15 *This configuration of a Michelson interferometer is known as a Twyman-Green. This configuration allows the interferometer to test an arbitrary optical system that returns a wavefront that matches the wavefront of the reference (which, in the case shown, is a flat reference mirror).*

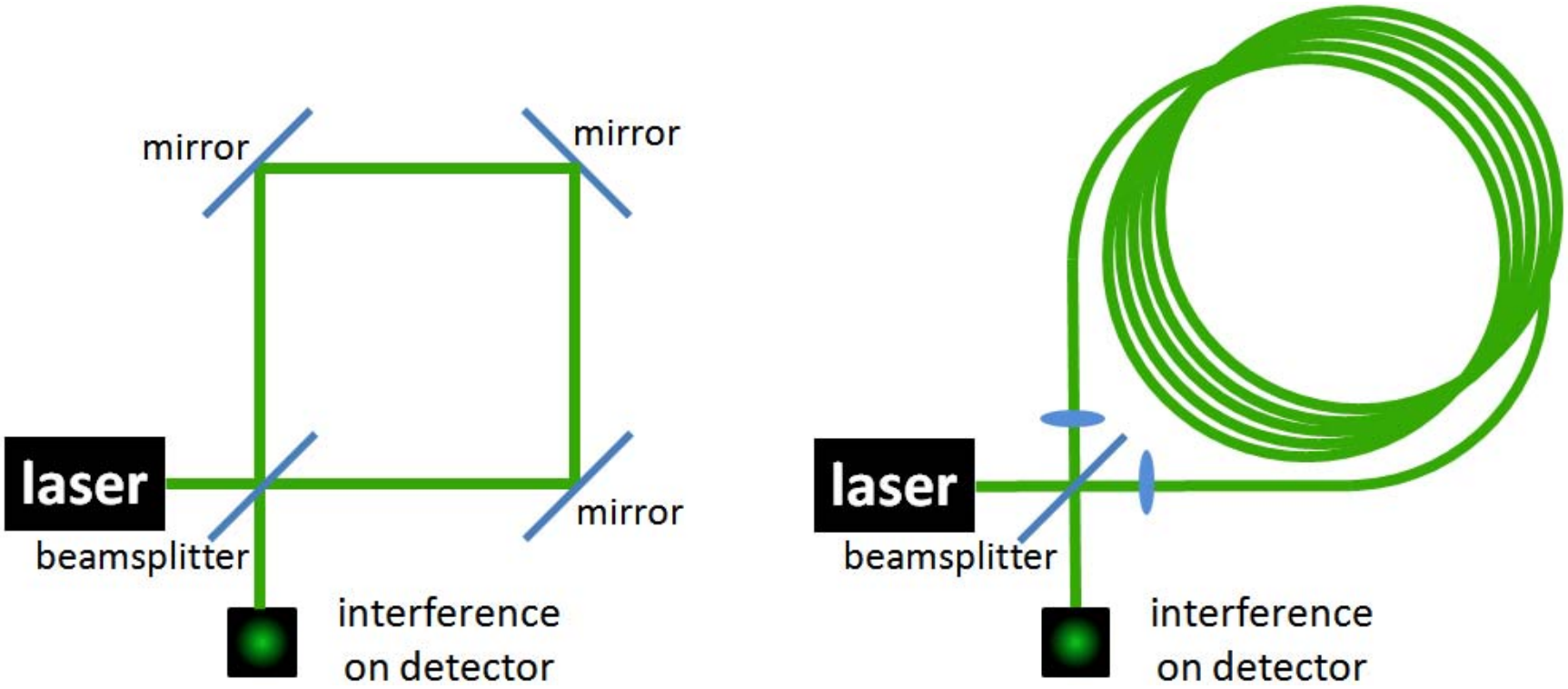

Figure 3-16 *The schematic on the left shows a three-mirror ring Sagnac interferometer, but any number of mirrors can be used to close the loop. The schematic on the right shows the Sagnac interferometer geometry as light propagates in opposite directions through a coil of optical fiber. Rotation of either ring creates a phase shift and, therefore, interference.*

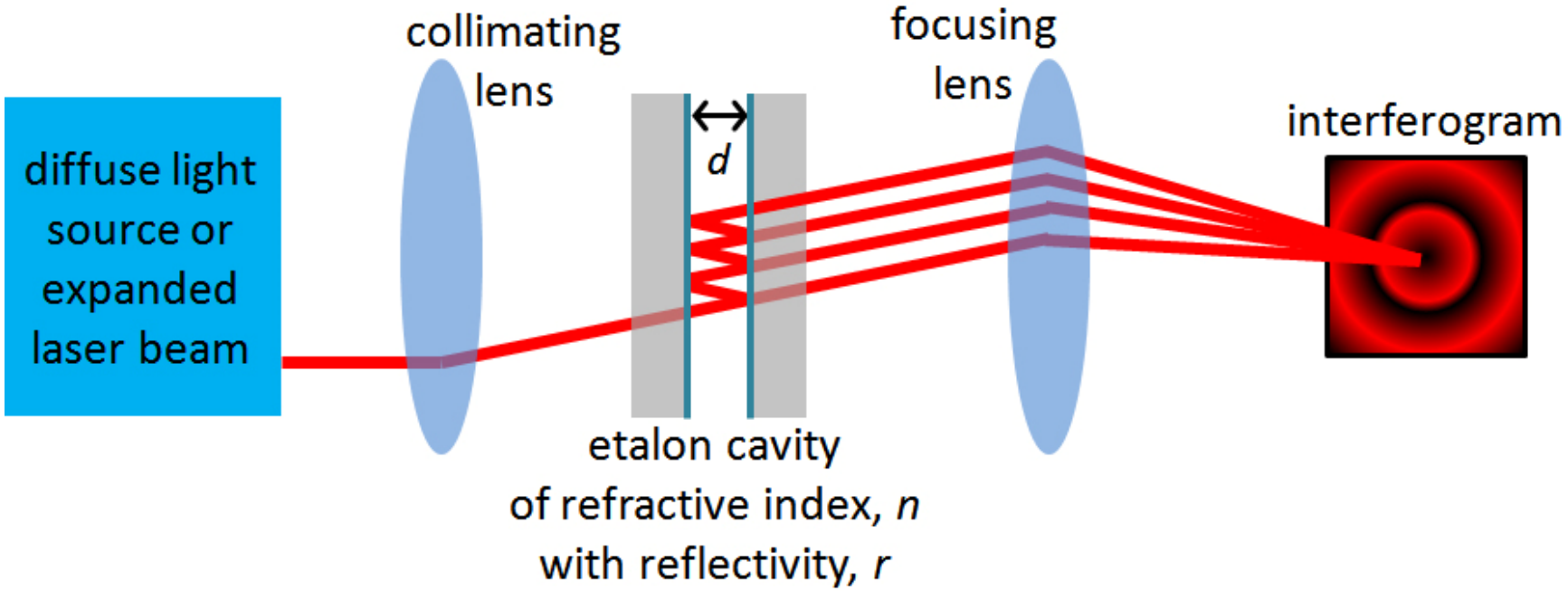

Figure 3-17 *An extended, diffuse source or an expanded laser can illuminate a Fabry-Perot interferometer (or etalon) cavity as shown, using a second lens to localize fringes on a screen.*

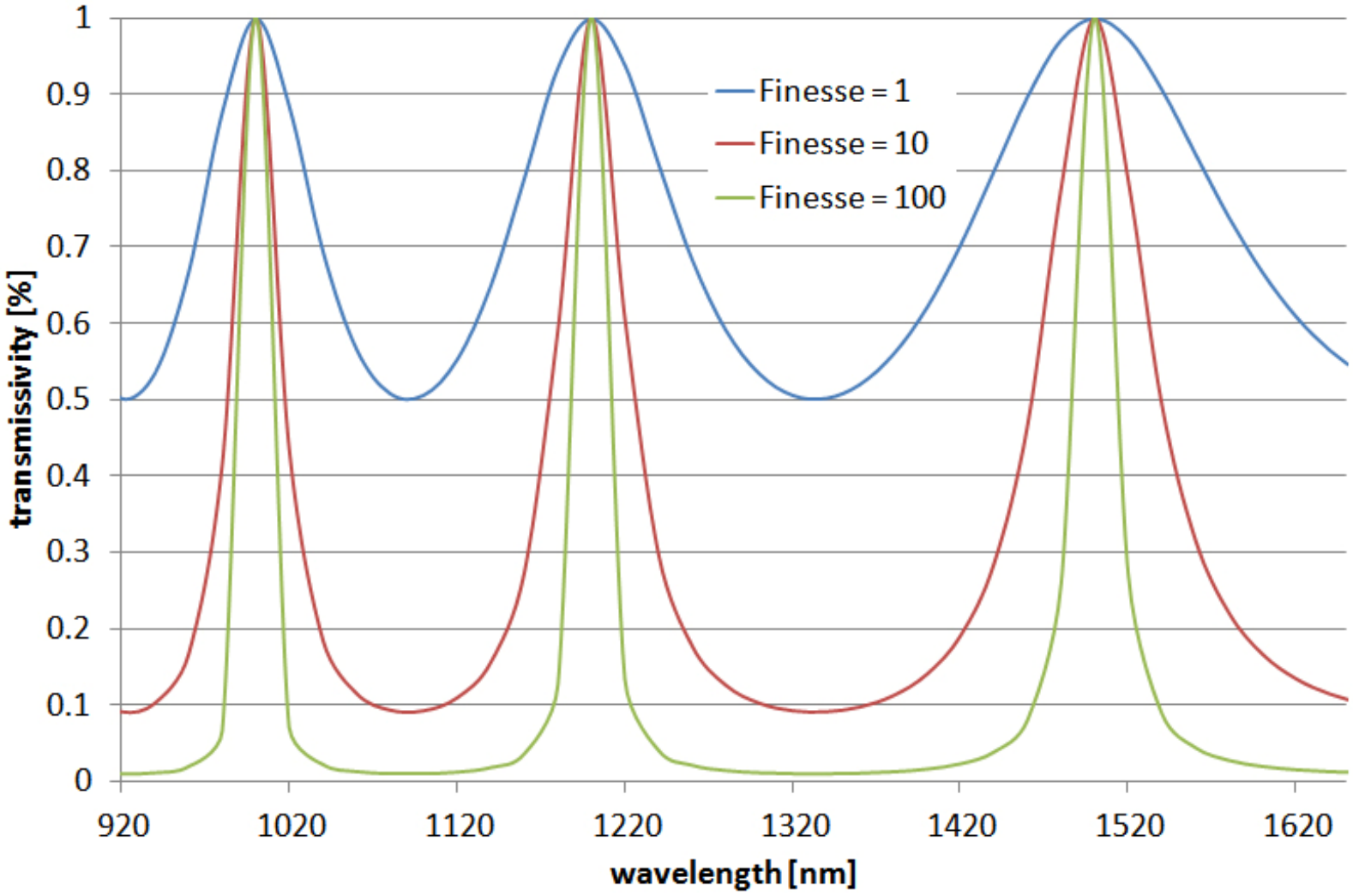

Figure 3-18 *These plots show the characteristic performance of an etalon for various values of finesse from 1 to 100. It is evident that the higher the finesse, the narrower the spectral resolution. However, higher finesse leads to lower light transmission.*

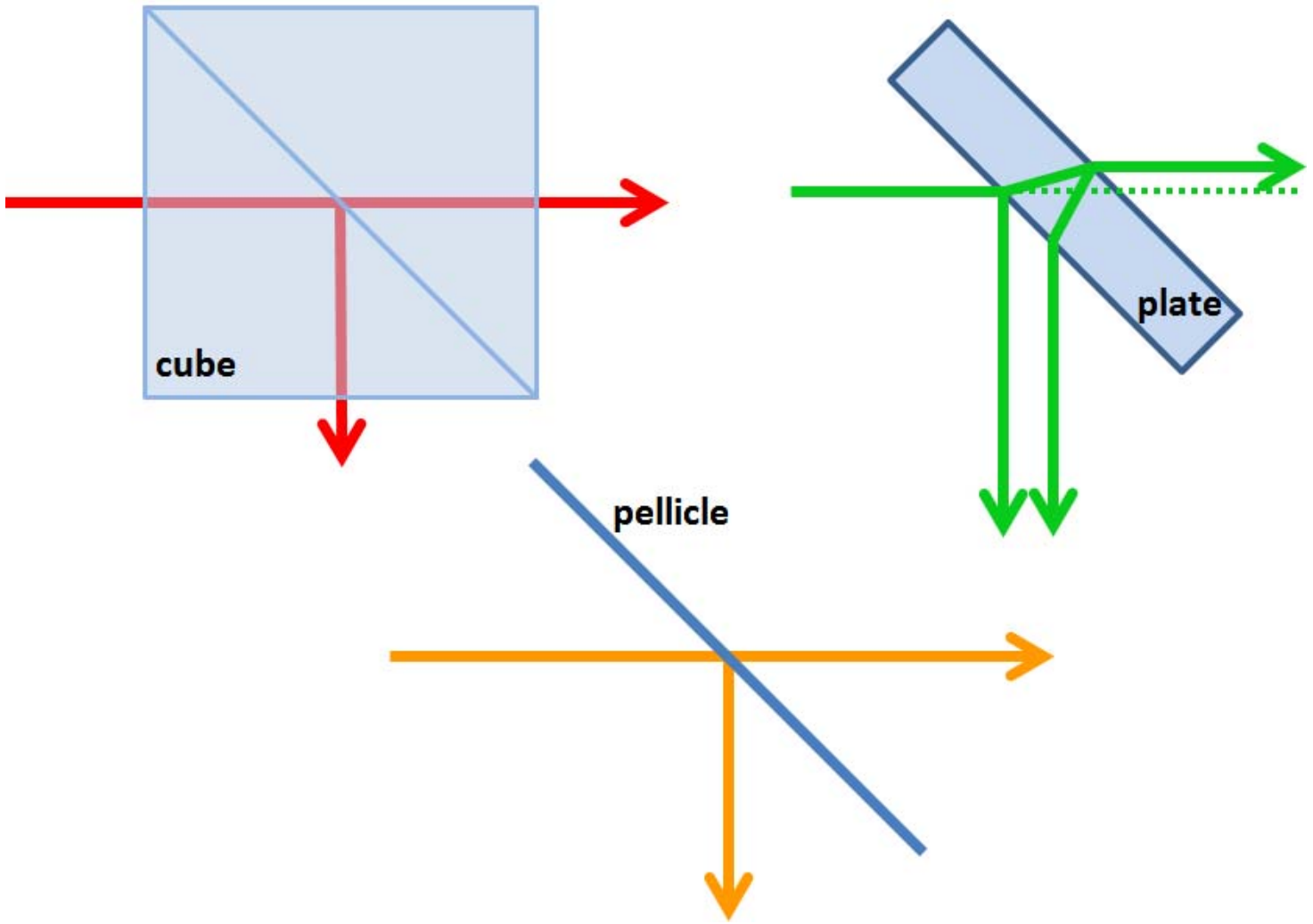

Figure 3-19 *This schematic shows three types of beamsplitters common to interferometers: cube, plate, and pellicle.*

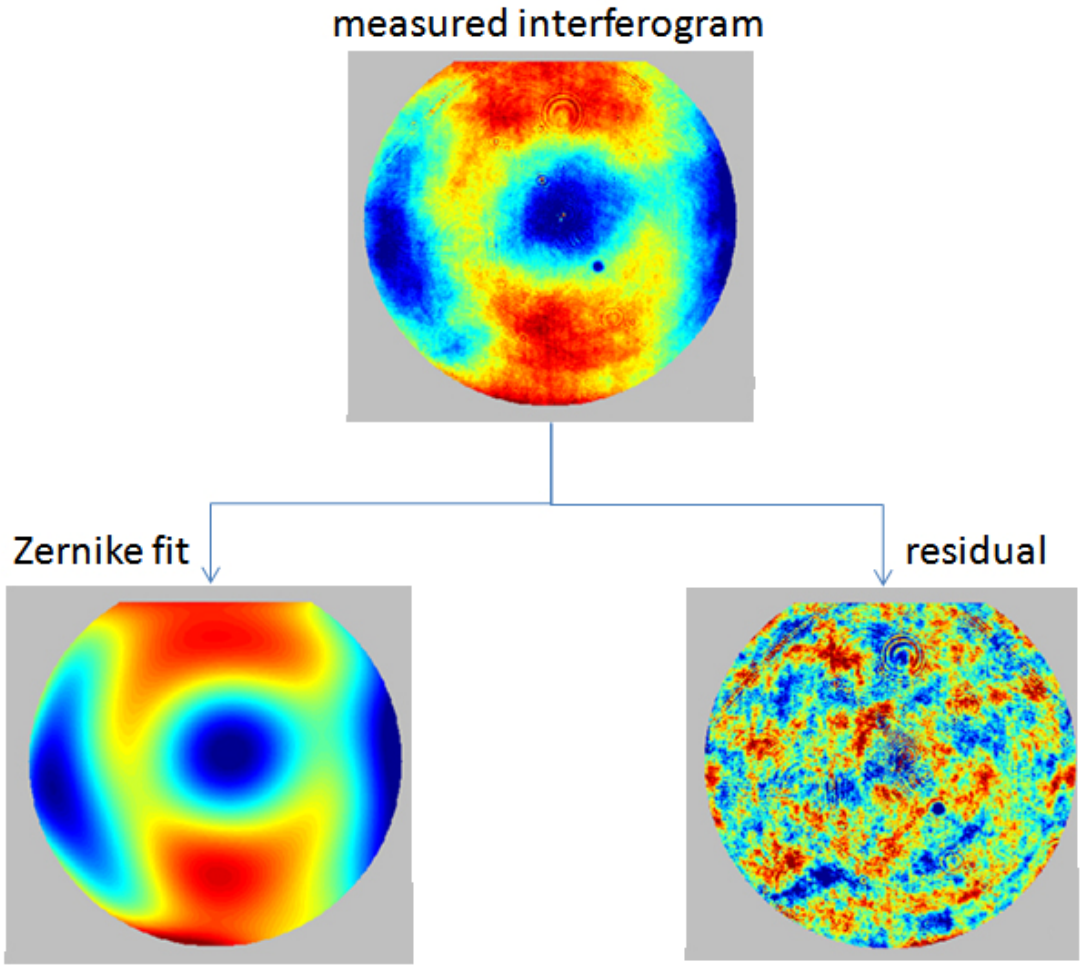

Figure 3-20 *This figure shows a measured interferogram (top), along with a 36-term mathematical Zernike polynomial fit (lower left) and the residual WFE map (lower right) that results.*

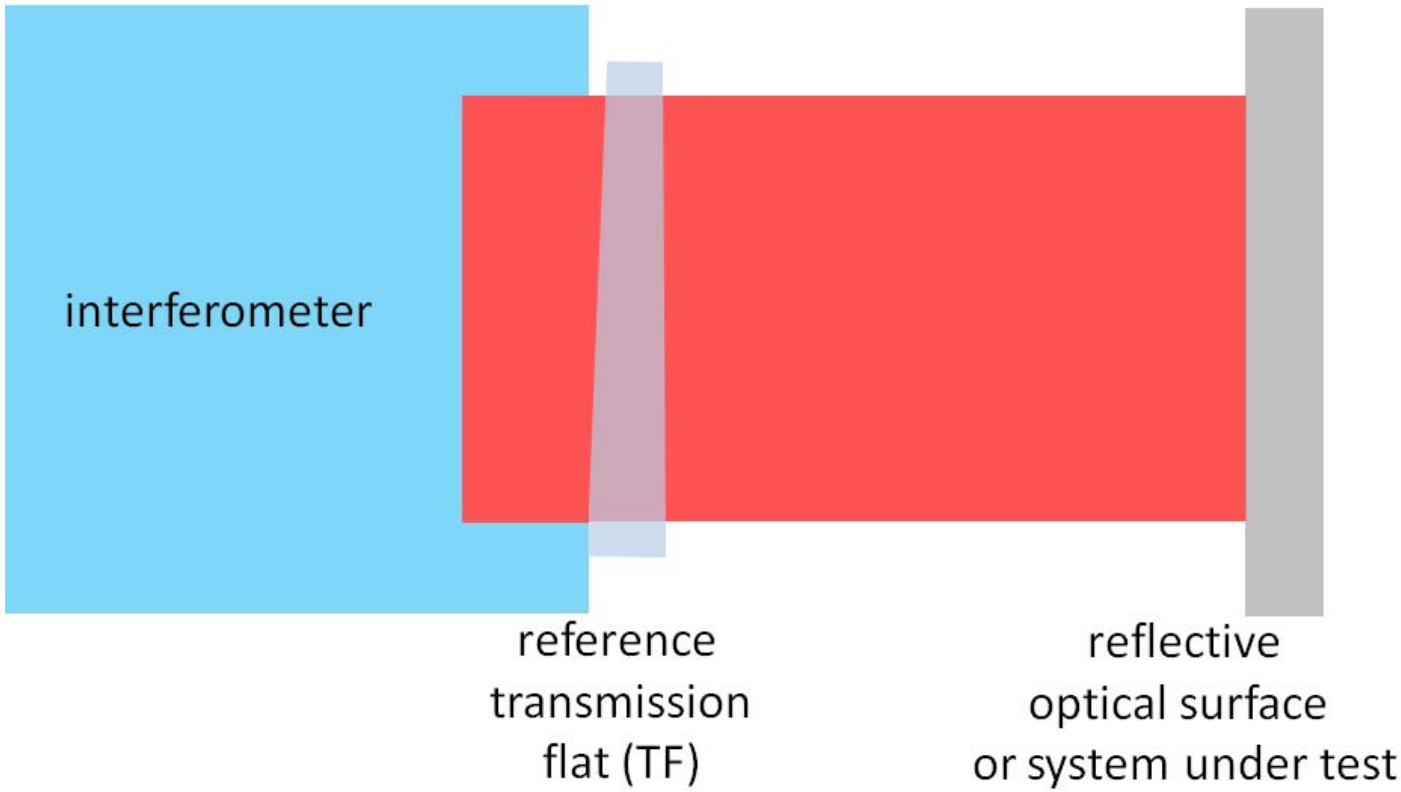

Figure 3-21 *This setup could be used to measure the RWFE of a flat mirror.*

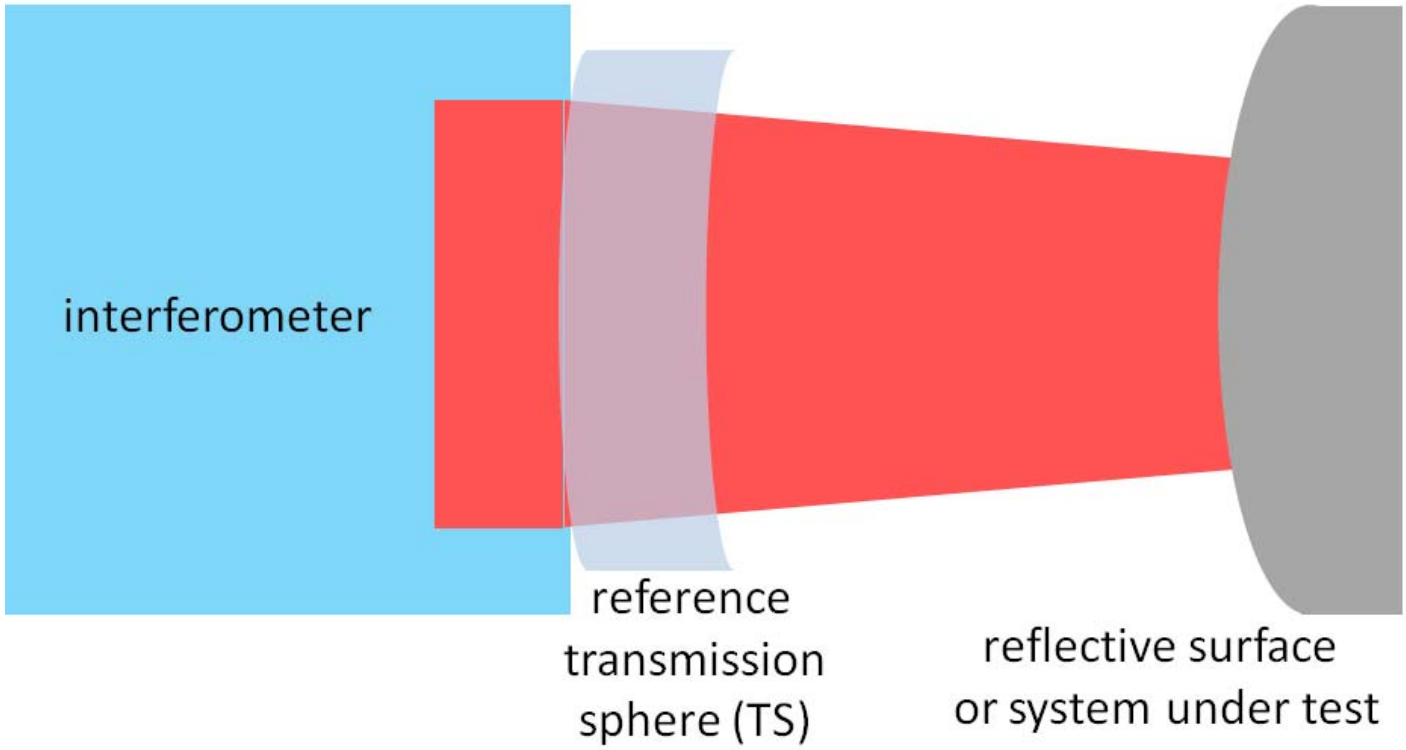

Figure 3-22 *This setup could be used to measure the surface figure or RWFE of a reflective optical system. This setup would be used to measure convex mirror surfaces or the RWFE of optical systems that diverge a beam upon reflection.*

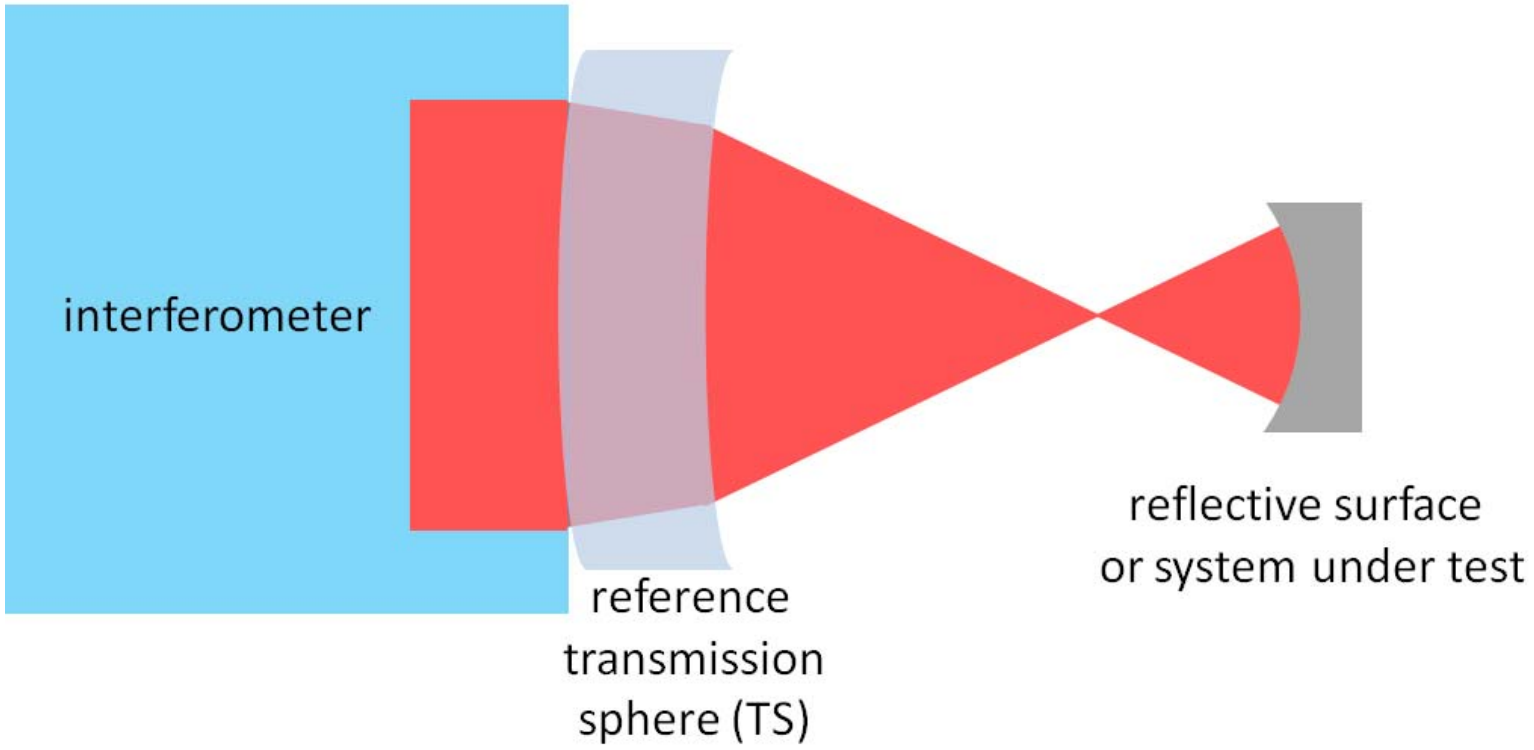

Figure 3-23 *This setup could also be used to measure the surface figure or RWFE of a reflective optical system. This setup would be used to measure concave mirror surfaces or the RWFE of optical systems that converge a beam upon reflection.*

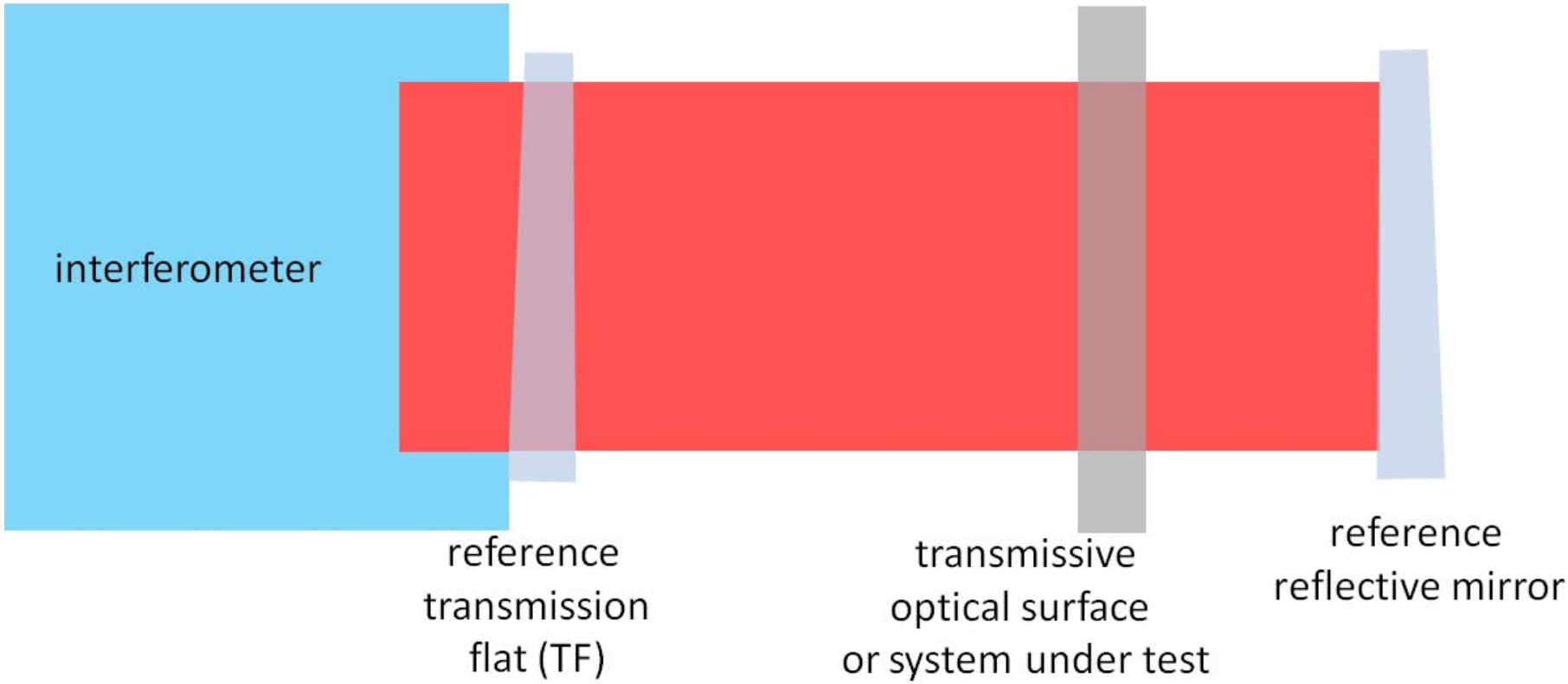

Figure 3-24 *This setup could be used to measure the TWFE of a transmissive optical system.*

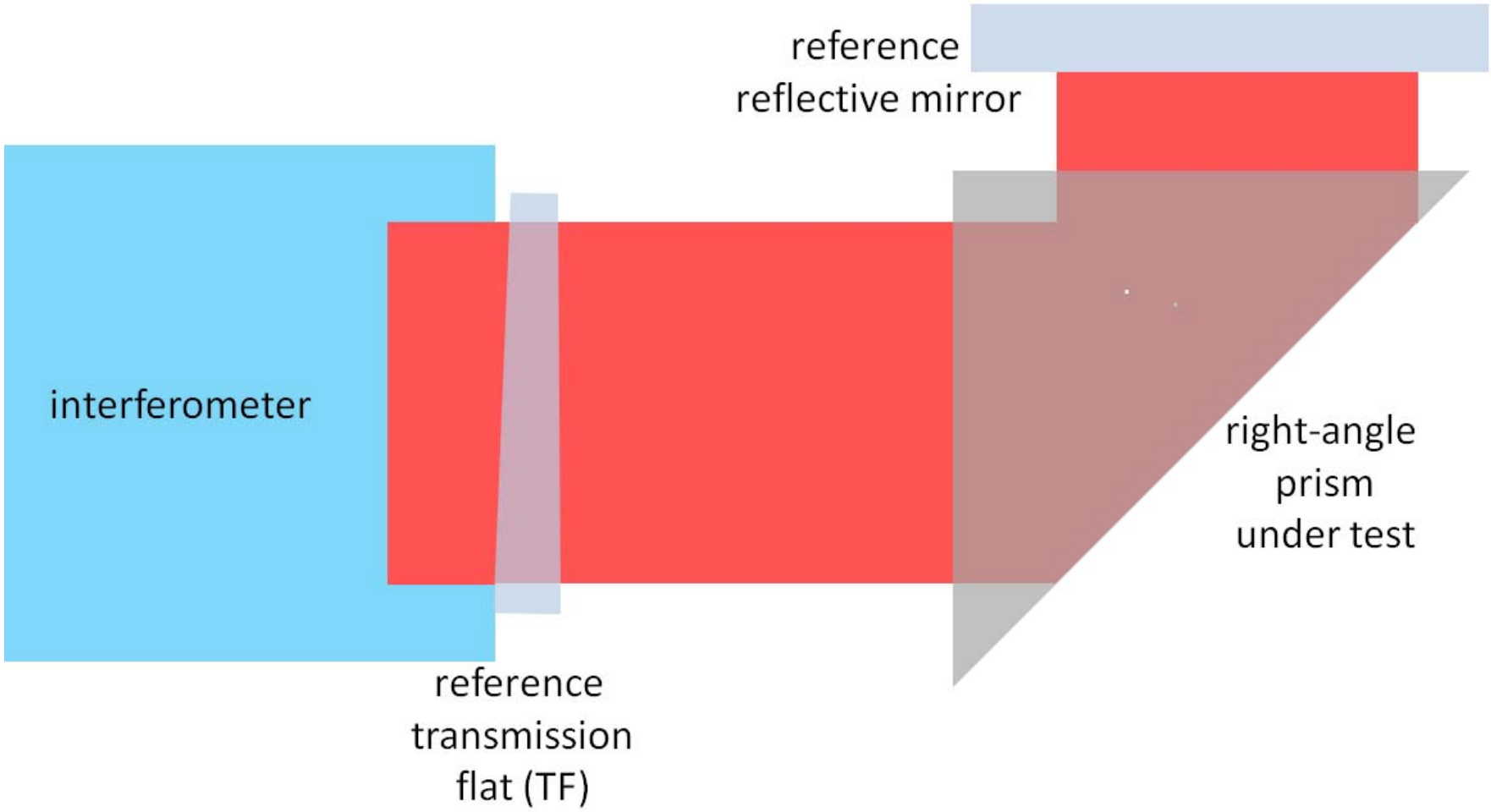

Figure 3-25 *This setup is an example of an application of the setup shown in Figure 3-24. In this figure, the generic transmissive optical system is replaced with a right-angle prism.*

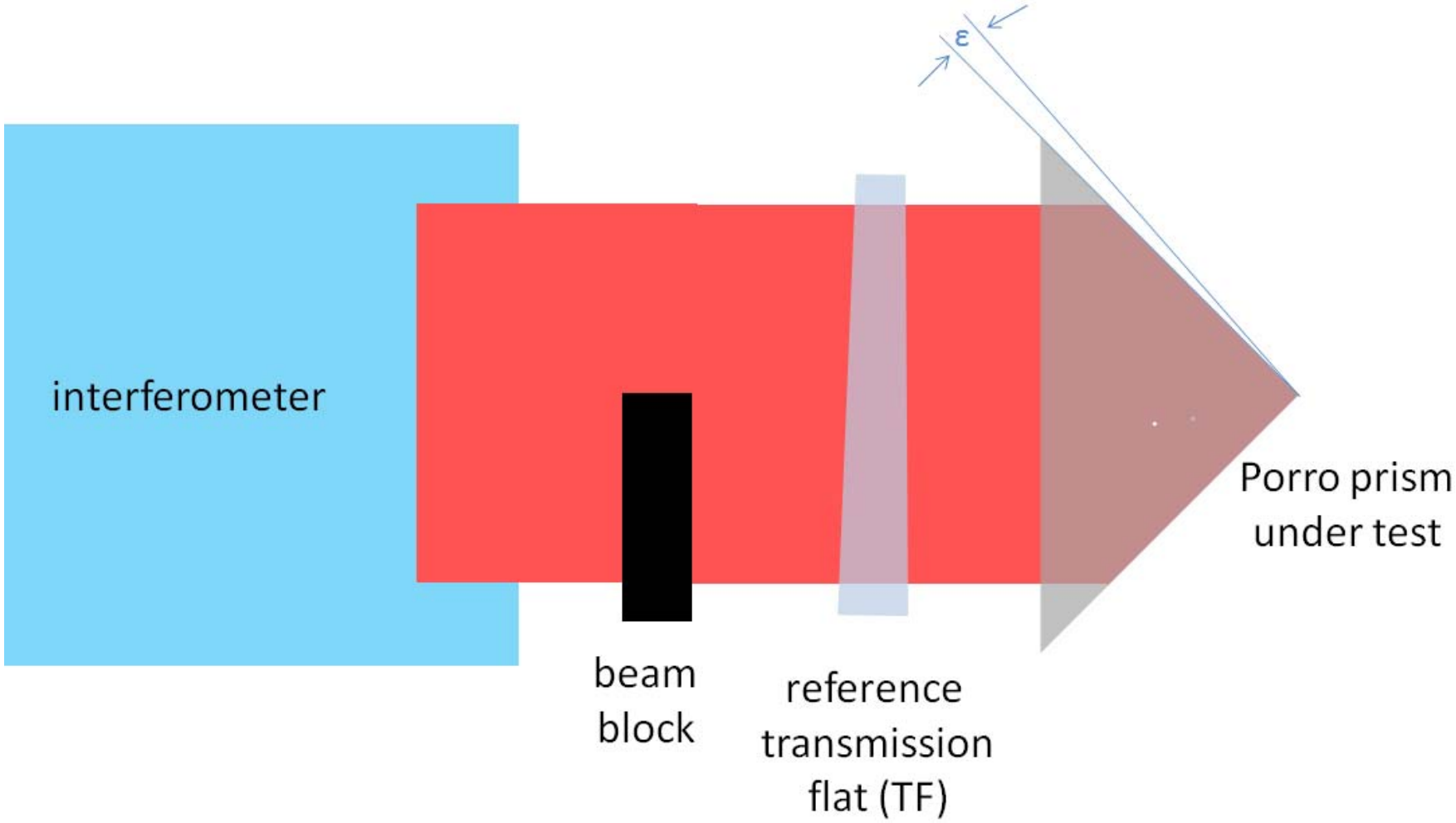

Figure 3-26 *This figure shows an interferometric test setup used to measure a prism's apex angle error in the Porro configuration via a Twyman-Green or Fizeau interferometer.*

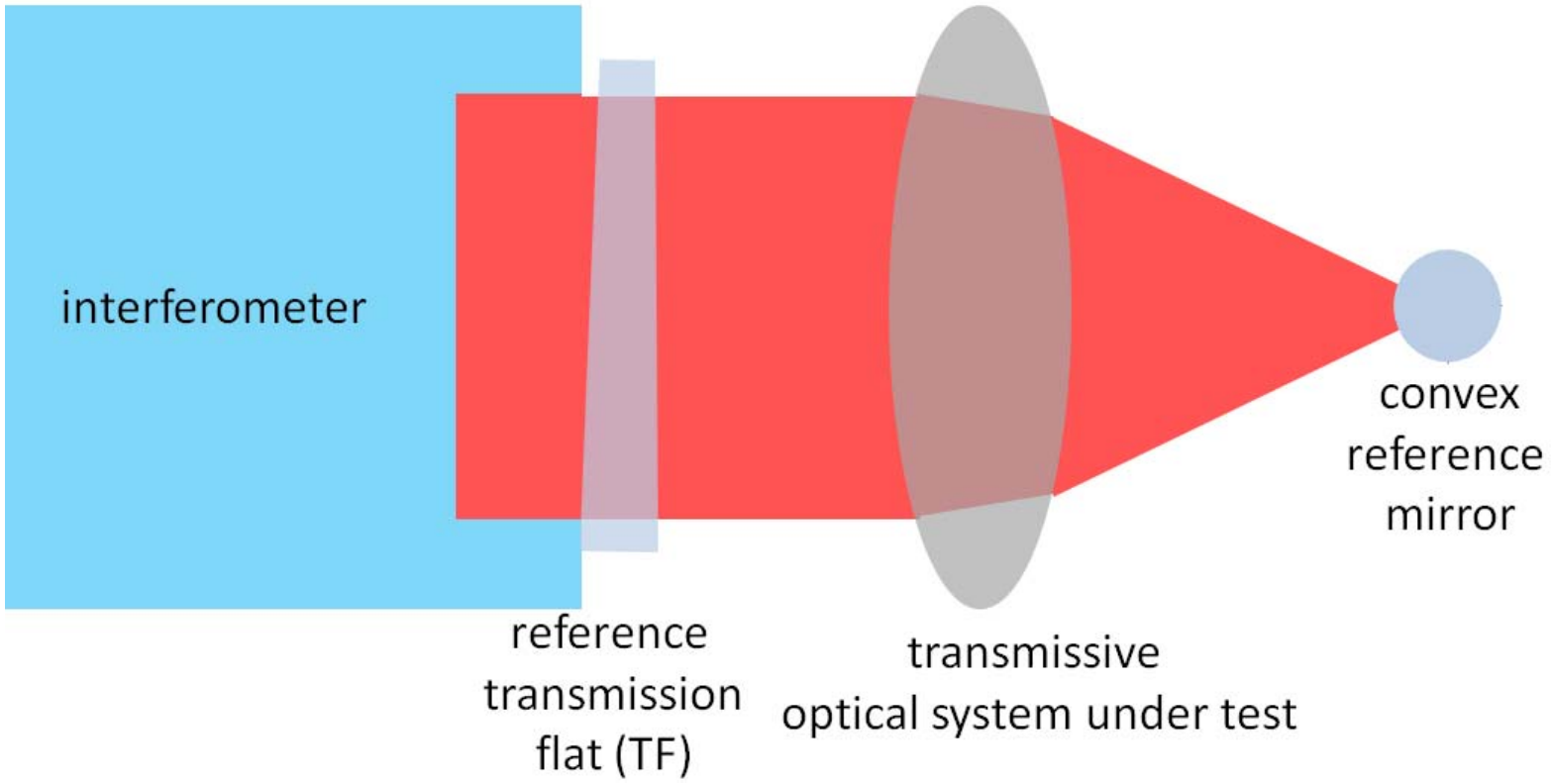

Figure 3-27 *This setup could be used to measure the TWFE of a transmissive optical system that converges a beam.*

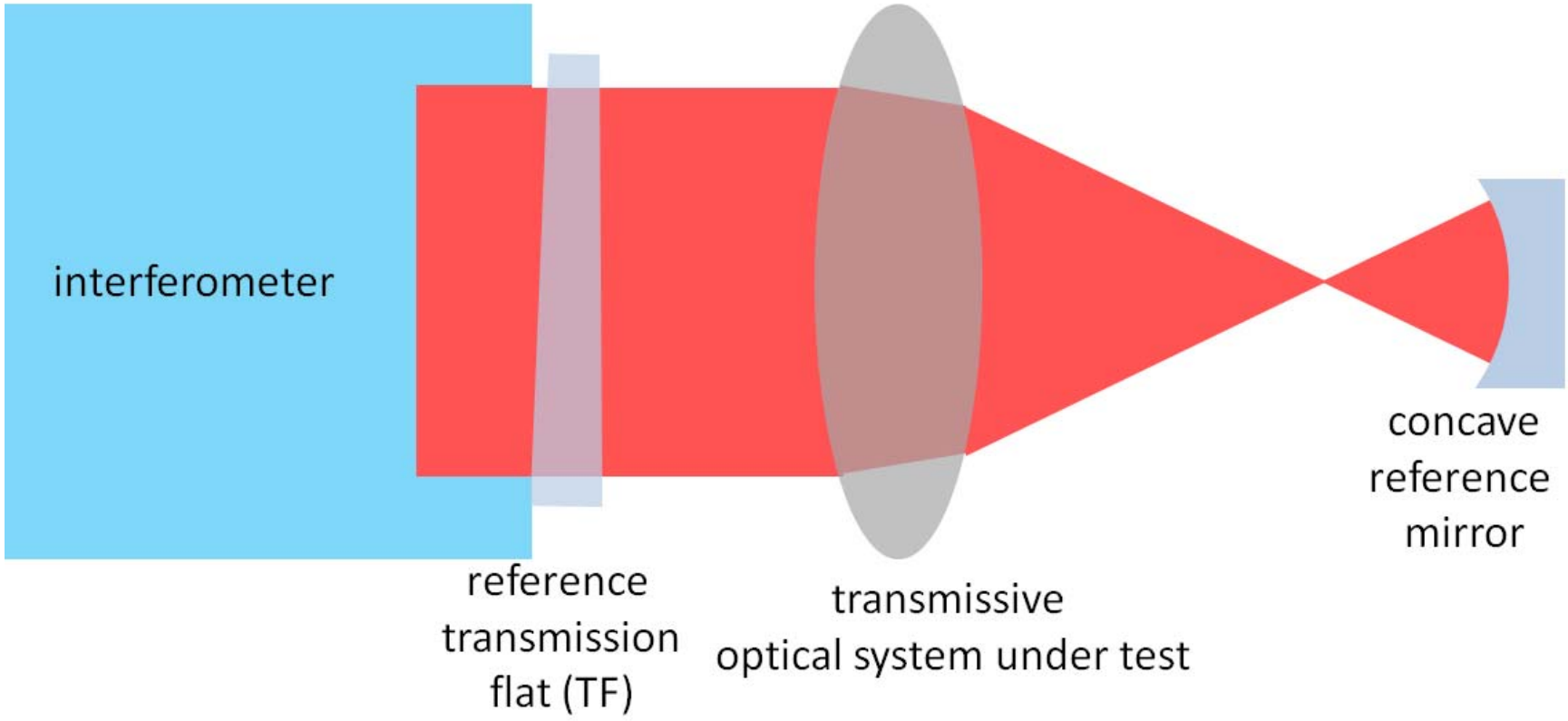

Figure 3-28 *This setup could also be used to measure the TWFE of a transmissive optical system that converges or diverges a beam.*

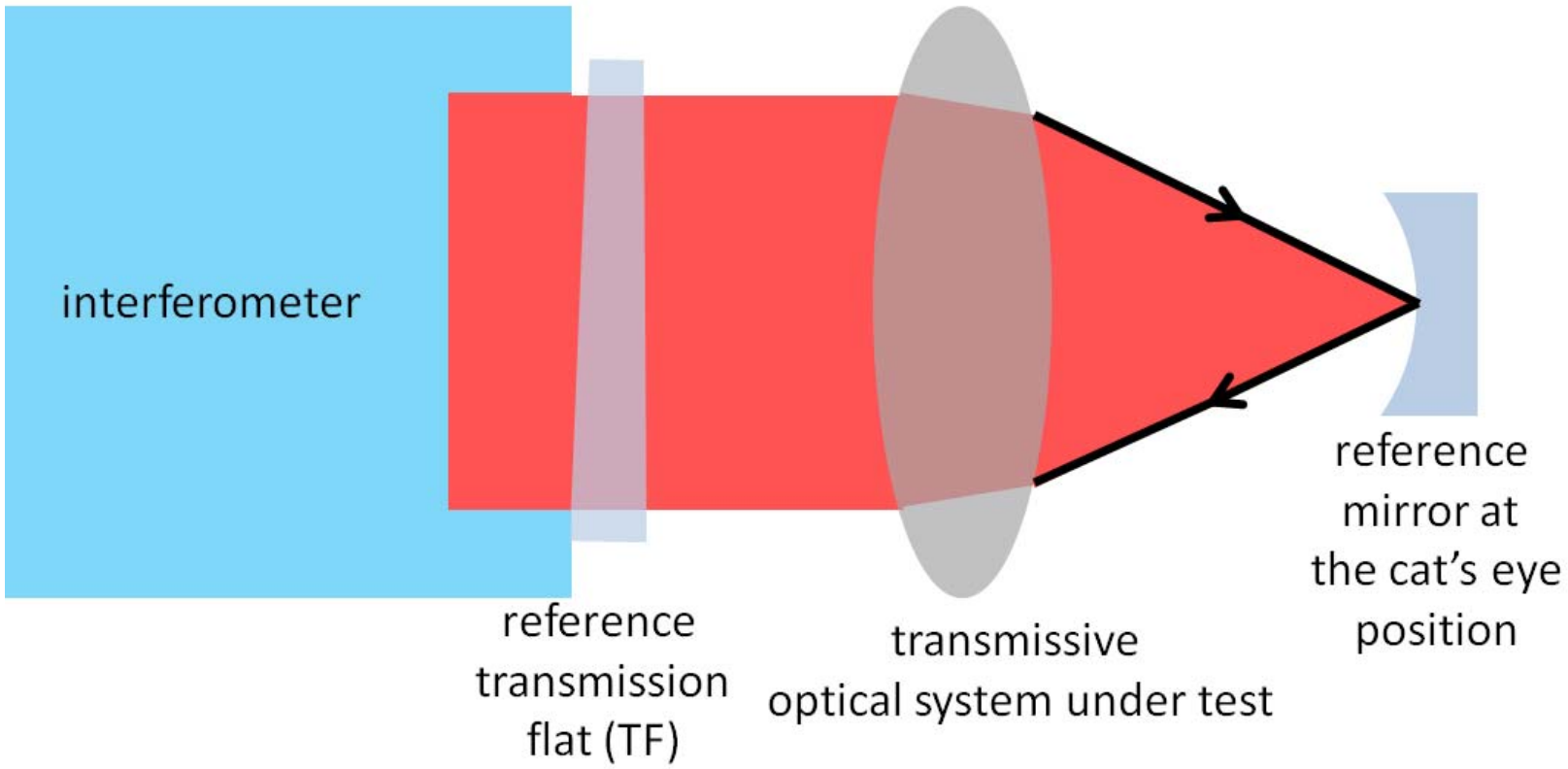

Figure 3-29 *Illustrated here is the light path taken when a reference optic is located at the cat's-eye position. Interference will occur from this configuration, and it must be understood so that it can be used or avoided during interferometric testing.*

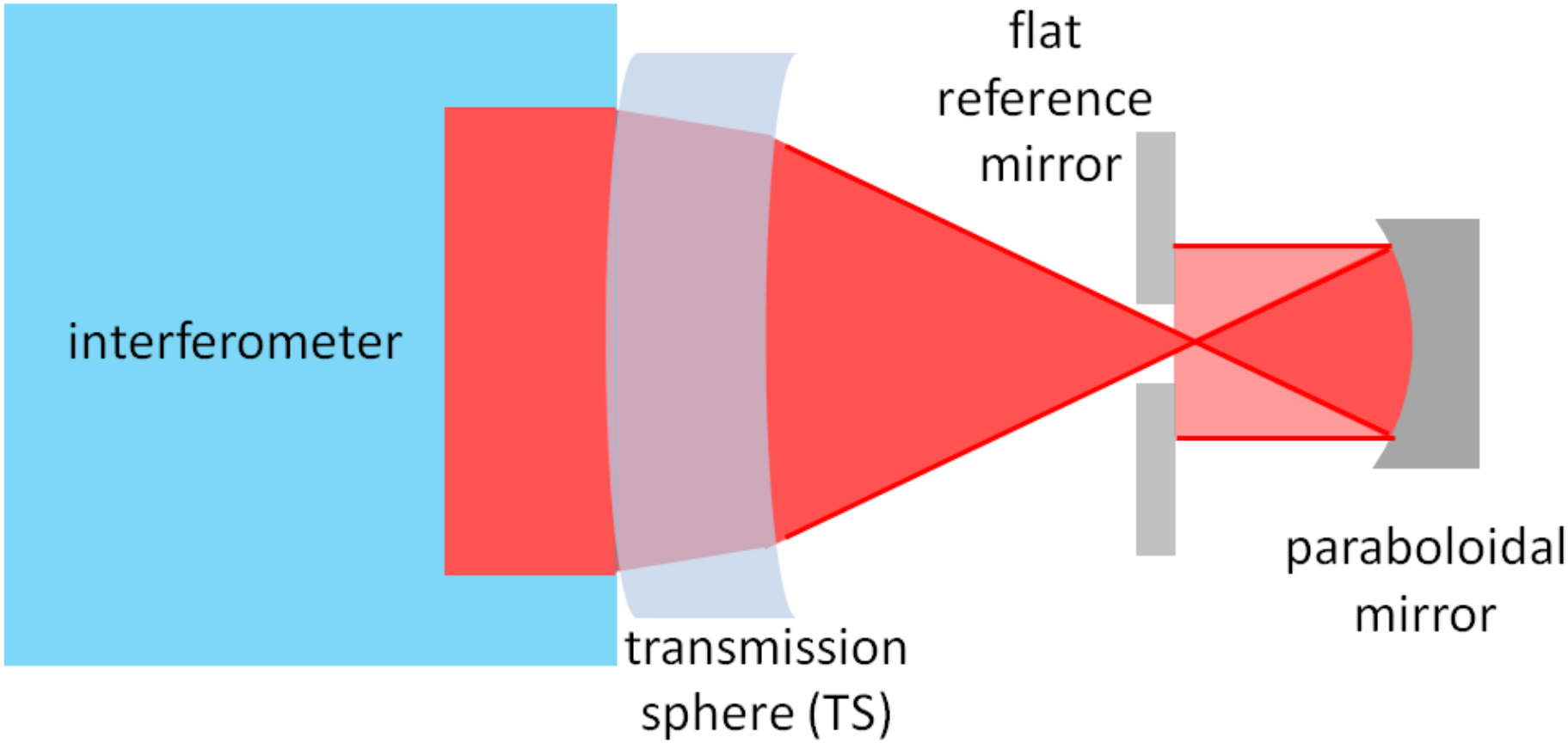

Figure 3-30 *Illustrated here is the light path taken when a flat reference mirror is used to test a paraboloidal surface.*

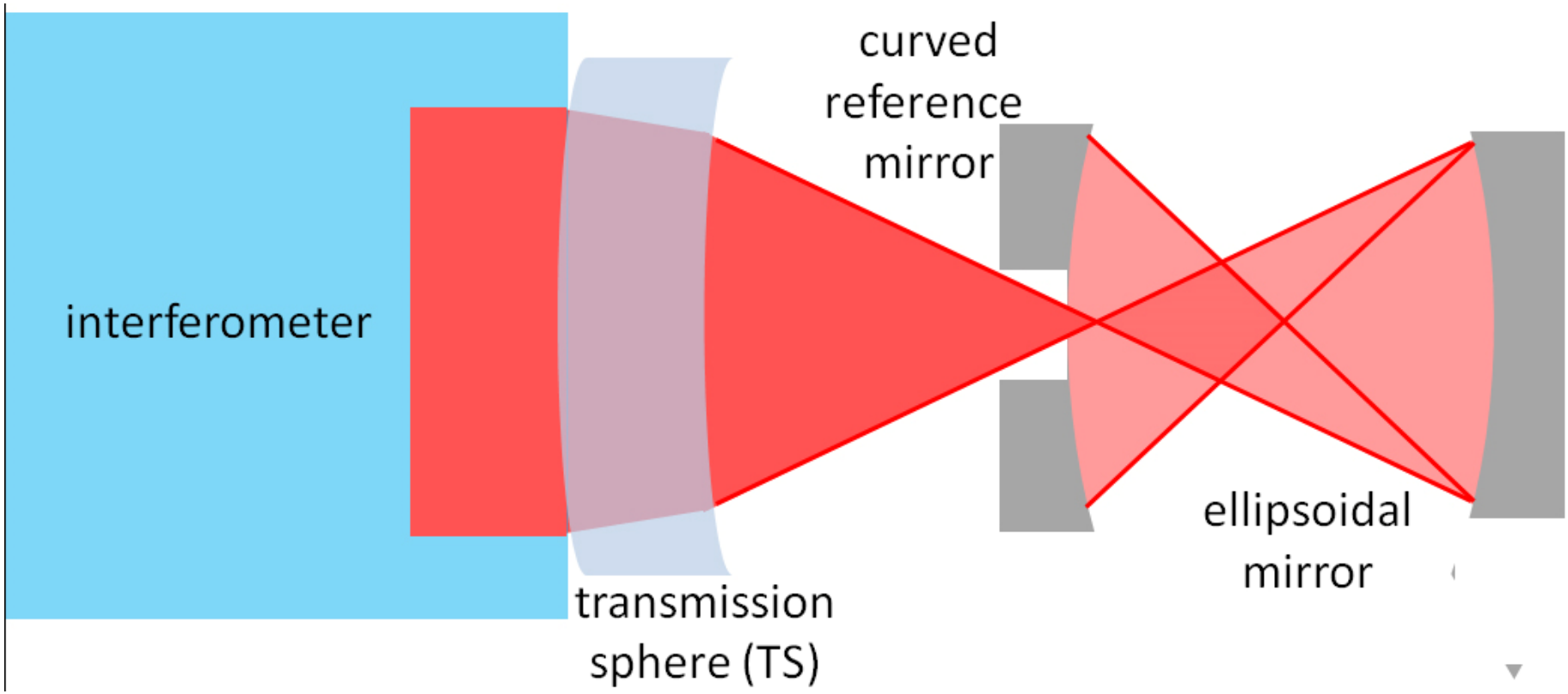

Figure 3-31 *Illustrated here is the light path taken when a curved reference mirror is used to test a ellipsoidal surface.*

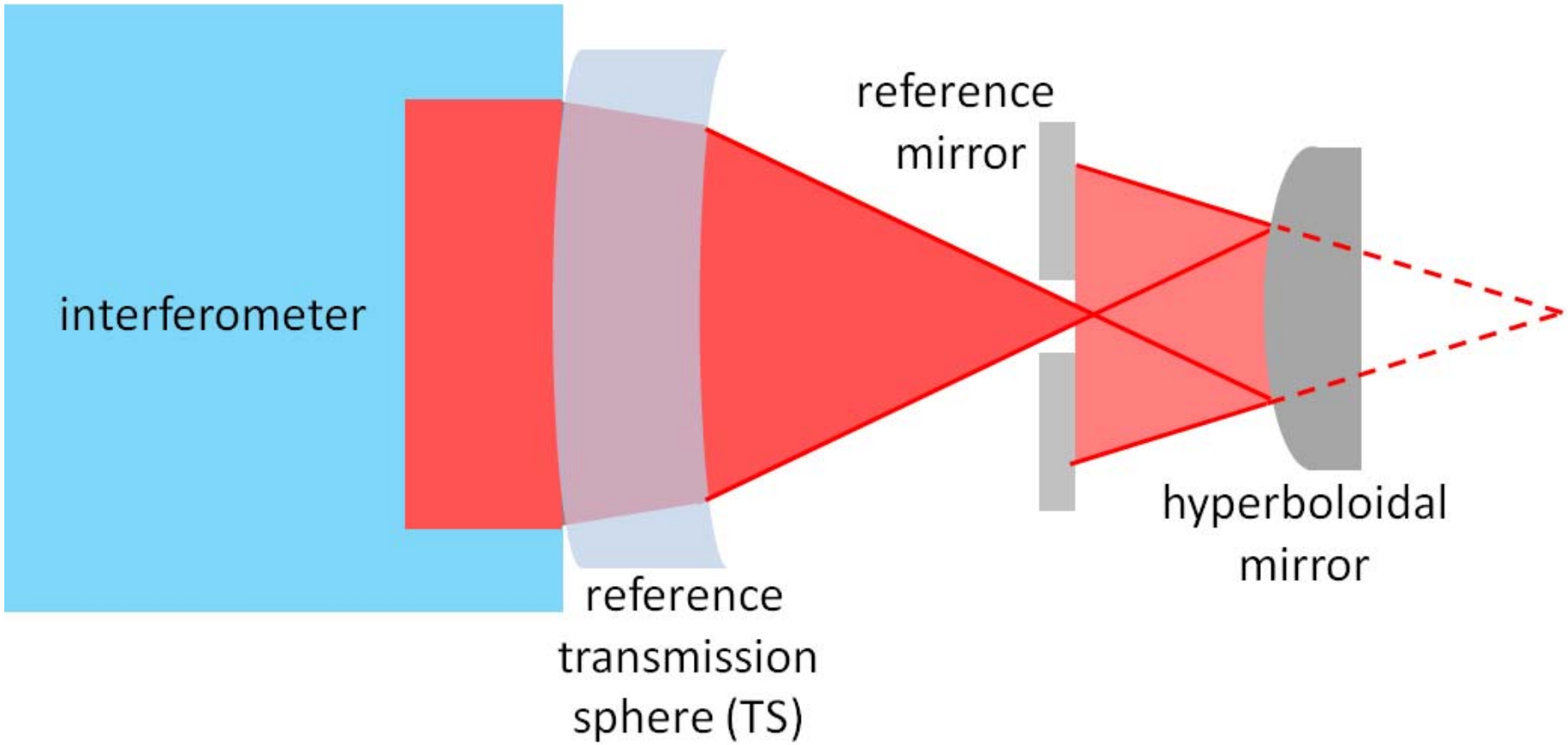

Figure 3-32 *Illustrated here is the light path taken when a reference transmission sphere is used to test a hyperboloidal surface.*

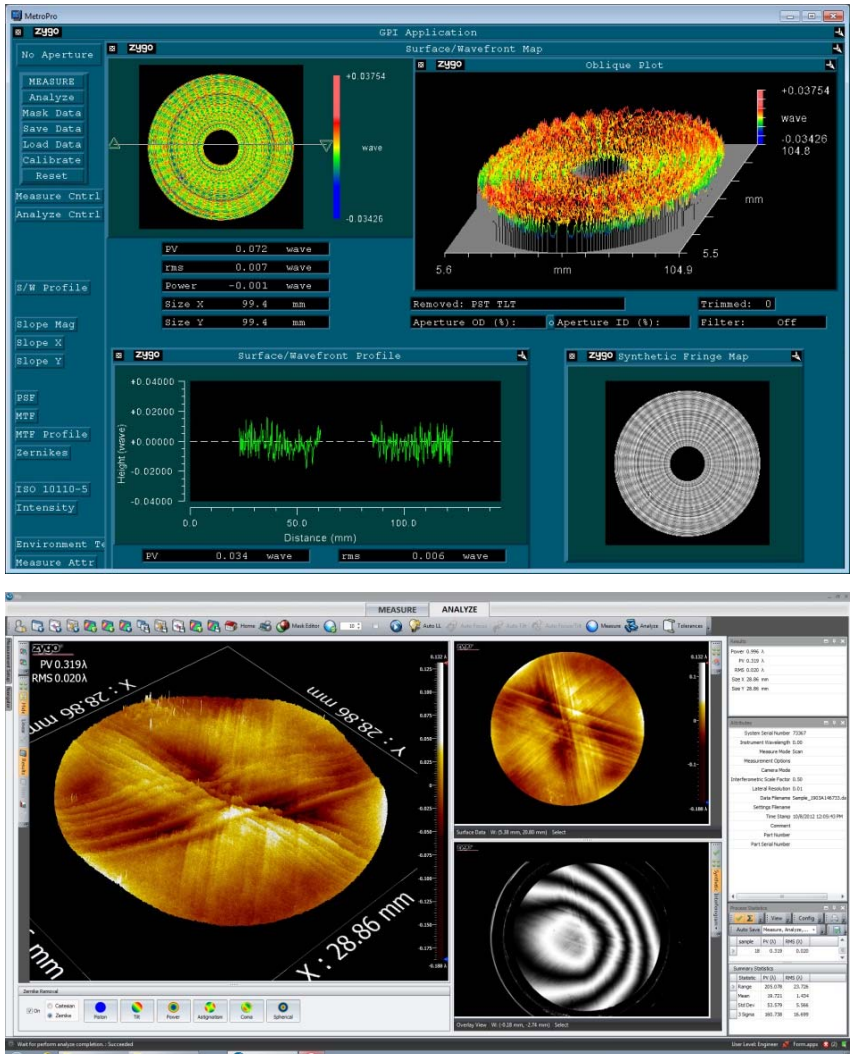

Figure 3-33 *These screenshots from Zygo's MetroPro software show a diamond-turned telescope mirror on the top (MetroPro 9) and a crystalline CO_2 laser optic on the bottom (MetroPro X). The raw (wrapped) fringe measurements can be seen in the lower right portions of both images.*

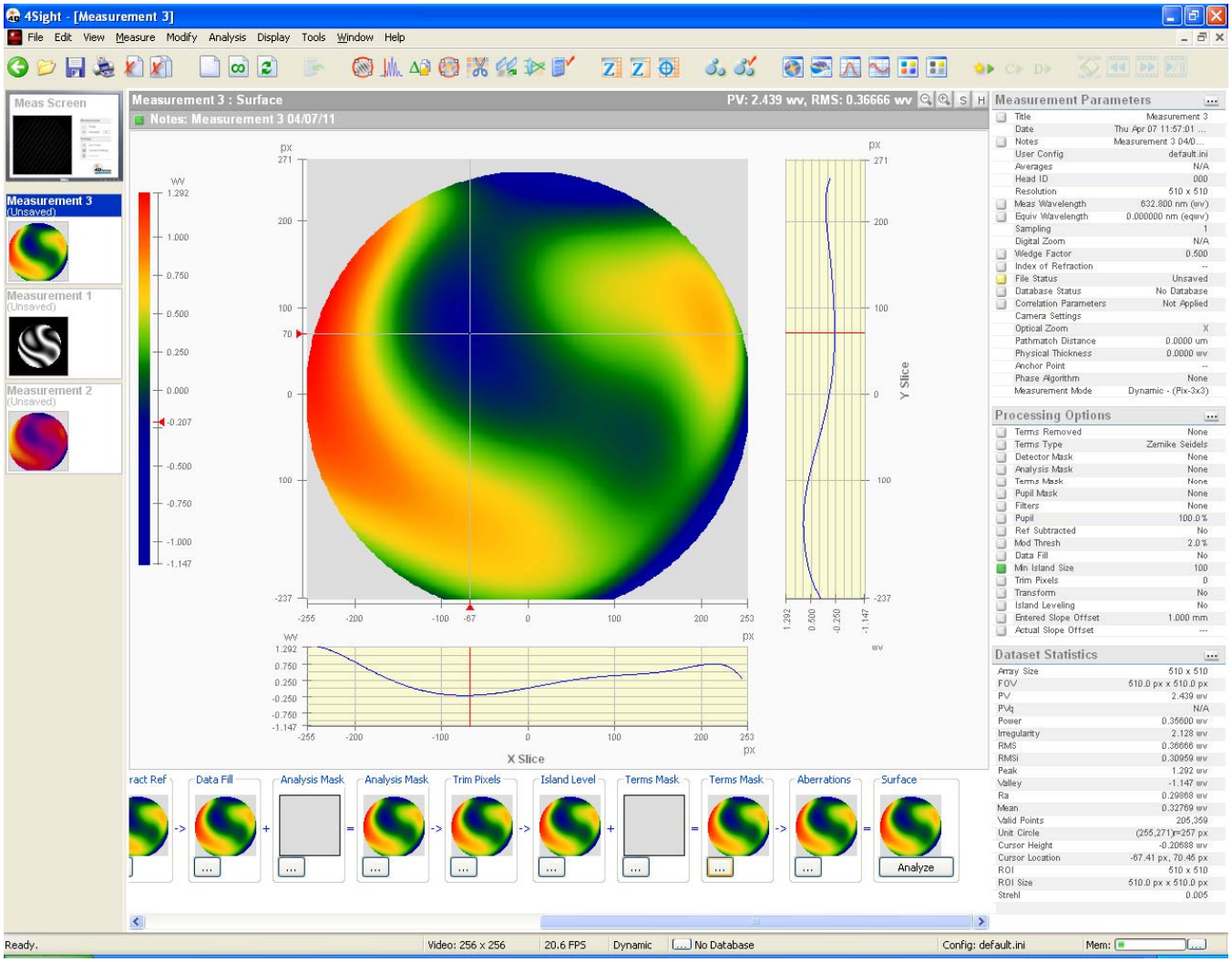

Figure 3-34 *This screenshot from 4D's 4Sight software shows an unwrapped interferogram and the wavefront metrics for this measurement. In fact, the raw (wrapped) fringe measurement can be seen in the smaller image on the left side of the screenshot.*

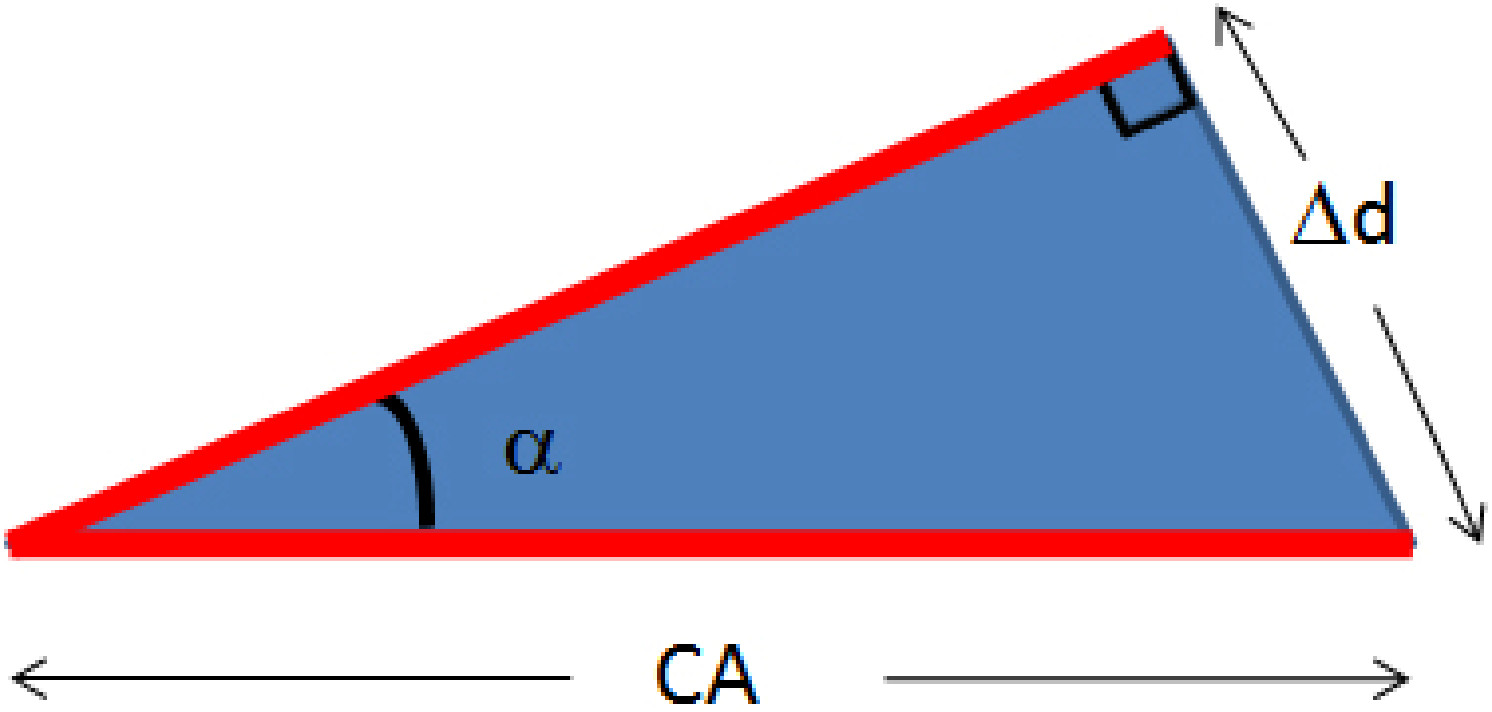

Figure 3-35 *The bold lines represent the position of a mirror in a Michelson interferometer before and after it is tilted by distance Δd to angle α. CA is the clear aperture of the beam on the tilted mirror.*

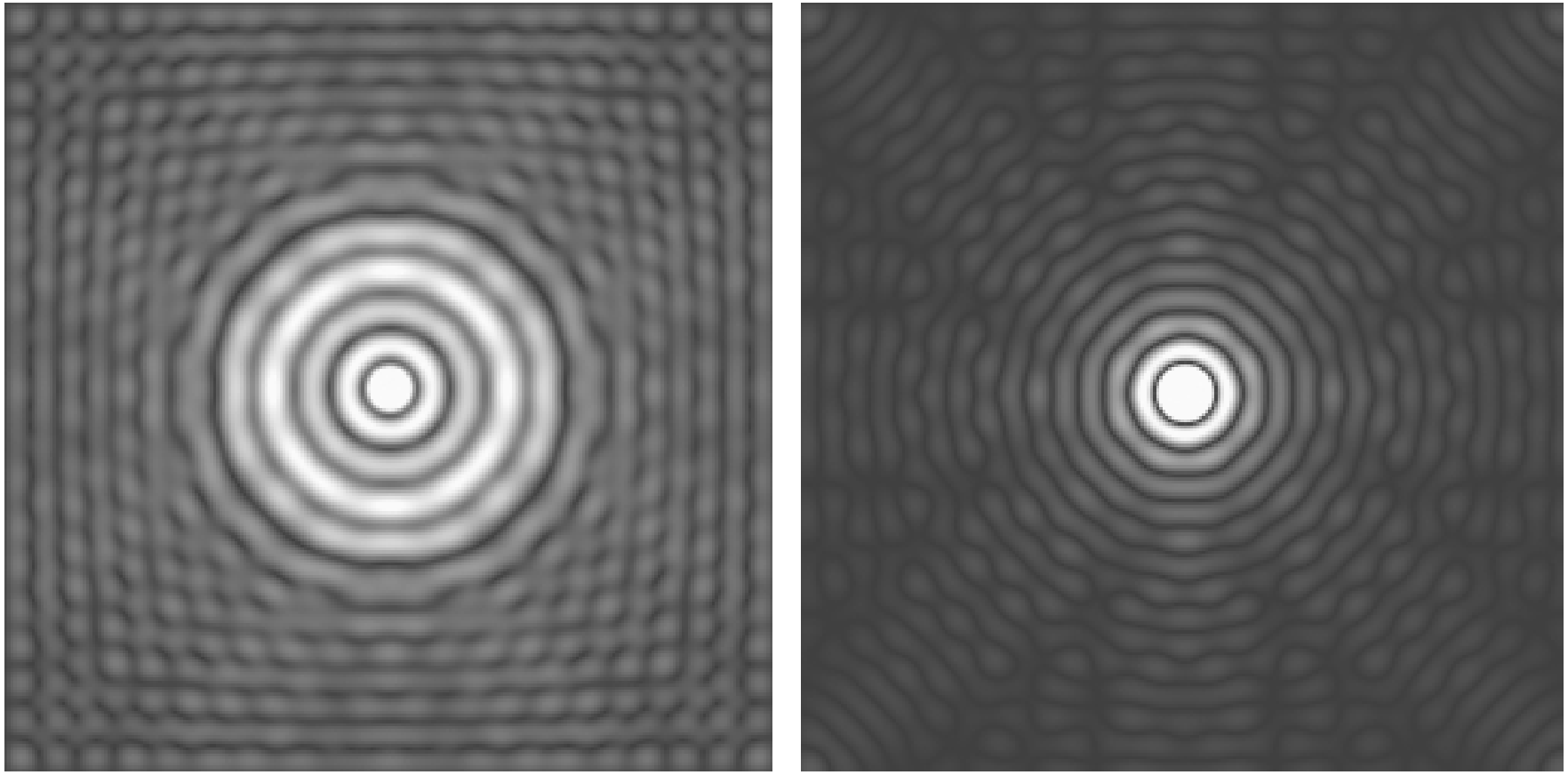

Figure 3-36 *The spots formed by an optical system with spherical aberration (left) that is compensated by defocus (right).*

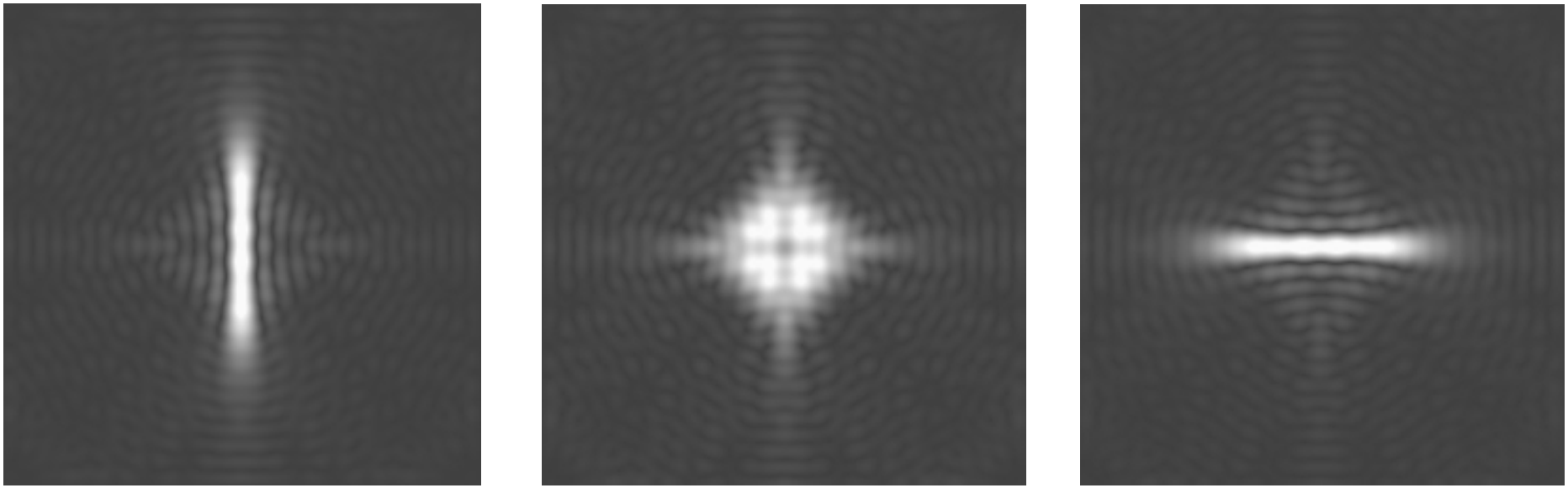

Figures 3-37 *As the astigmatic optical system is defocused from the tangential (left) to the saggital (right) focal line, the circle of least confusion can be observed.*

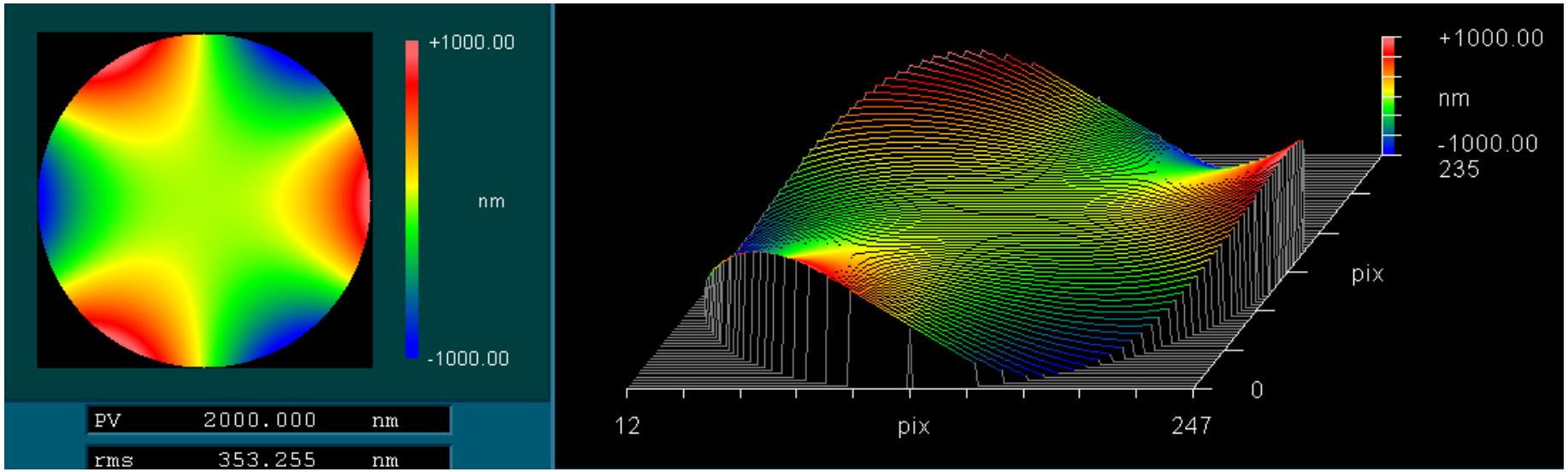

Figure 3-38 *This interferogram is indicative of a three-point mounting aberration.*